JOURNAL OF PETROLOGY | VOLUME 41 | NUMBER 1 | PAGES 87–109 | 2000

The Cameroon Volcanic Line Revisited: Petrogenesis of Continental Basaltic Magmas from Lithospheric and Asthenospheric Mantle Sources

A. MARZOLI[1,2]*, E. M. PICCIRILLO[1], P. R. RENNE[2,3], G. BELLIENI[4], M. IACUMIN[1], J. B. NYOBE[5] AND A. T. TONGWA[6]

[1]DIPARTIMENTO DI SCIENZE DELLA TERRA, UNIVERSITY OF TRIESTE, VIA E. WEISS 8, 34127 TRIESTE, ITALY

[2]BERKELEY GEOCHRONOLOGY CENTER, 2455 RIDGE ROAD, BERKELEY, CA 94709, USA

[3]DEPARTMENT OF GEOLOGY AND GEOPHYSICS, UNIVERSITY OF CALIFORNIA, BERKELEY, CA 94720, USA

[4]DIPARTIMENTO DI MINERALOGIA E PETROLOGIA, UNIVERSITY OF PADOVA, CORSO GARIBALDI 37, 35137 PADOVA, ITALY

[5]MINISTÈRE DE RECHERCHE SCIENTIFIQUE TECHNOLOGIQUE, B.P. 4110, YAOUNDÉ, CAMEROON

[6]LABORATORY FOR EARTHQUAKE CHEMISTRY, UNIVERSITY OF TOKYO, HONGO BUNKYO-KU, TOKYO 113, JAPAN

RECEIVED OCTOBER 5, 1998; REVISED TYPESCRIPT ACCEPTED JUNE 24, 1999

The volcanic activity of Mts Bambouto and Oku (Western Highlands) and of the Ngaoundere Plateau, in the continental sector of the Cameroon Volcanic Line, Equatorial West Africa, ranges in age from Oligocene to Recent. It is characterized by basanitic, alkali basaltic and transitional basaltic series. Mineral chemistry, major and trace element bulk-rock compositions, and geochemical modelling suggest that the magmatic series evolved mainly at low pressure (2–4 kbar) through fractional crystallization of clinopyroxene and olivine ± magnetite, at moderately hydrated (H_2O = 0·5–1 wt %) and QFM (quartz–fayalite–magnetite) to QFM + 1 fO_2 conditions. Basalts from Ngaoundere (Miocene to Quaternary) and from the early activity (31–14 Ma) of the Western Highlands have incompatible trace element and Sr–Nd isotopic compositions similar to those of oceanic Cameroon Line basalts, pointing to a similar asthenospheric mantle source. By contrast, the late (15–4 Ma) Western Highlands basanites and alkali basalts have anomalously high concentrations of Sr, Ba and P, and low concentrations of Zr, which are exclusive features of continental Cameroon basalts. The genesis of these latter magmas is consistent with derivation from an incompatible element enriched, amphibole-bearing lithospheric mantle source. Western Highlands basalts show a continuous spectrum from high to low Sr–Ba–P compositions, and may result from variable amounts of mixing between melts derived from an anhydrous lherzolite source (asthenospheric component) and melts from an amphibole-bearing peridotite source (lithospheric HSr component). New $^{40}Ar/^{39}Ar$ ages for Mts Oku and Bambouto basalts, combined with previous $^{40}Ar/^{39}Ar$ and K/Ar ages of basaltic and silicic volcanics, and with volcanic stratigraphy, suggest a NE–SW younging of the peak magmatic activity in the Western Highlands. This SW younging trend, extending from the Oligocene volcanism in northern Cameroon (e.g. Mt Oku) to the still active Mt Cameroon, suggests that the African plate is moving above a deep-seated mantle thermal anomaly. However, the age and location of the Ngaoundere volcanism does not conform to the NE–SW younging trend, implying that the continental sector of the Cameroon Volcanic Line cannot be easily interpreted as the surface expression of a single hotspot system.

KEY WORDS: *Cameroon Line basalts; $^{40}Ar/^{39}Ar$ geochronology; lithospheric and asthenospheric mantle source; hotspot*

*Corresponding author. Present address: Section des Sciences de la Terre, Université de Genève, 13 rue des Maraîchers, 1211 Genève 4, Switzerland. Telephone: +41-22-7026697. Fax: +41-22-3205732. e-mail: marzoli@terre.unige.ch

INTRODUCTION

The role of the lithospheric mantle in the petrogenesis of continental basalts is difficult to evaluate, as its nature and composition are known to be highly variable, and not easily distinguishable from the asthenospheric mantle. Continental basalts have distinct geochemical signatures compared with mid-ocean ridge basalts (MORB), but exhibit many similarities to oceanic island basalts (OIB). Lithospheric contamination of the asthenospheric mantle may occur through lithospheric delamination (e.g. McKenzie & O'Nions, 1995) or through ancient subduction processes (e.g. Hofmann, 1988). On the other hand, there is increasing evidence that melts originating from the asthenosphere interact with the lithospheric mantle en route to the surface (Chazot *et al.*, 1996; Wulff-Pedersen *et al.*, 1996; Class & Goldstein, 1997). Current debate concerns whether continental basalts are primarily derived from the asthenospheric mantle, and contaminated by lithospheric mantle, or if they originate from variably 'metasomatized' lithospheric mantle (e.g. Menzies & Hawkesworth, 1987; Francis & Ludden, 1995; Wulff-Pedersen *et al.*, 1996; Comin-Chiaramonti *et al.*, 1997).

An exceptional opportunity to determine the contribution of lithospheric mantle to the petrogenesis of alkali basalts is presented by the Tertiary–Quaternary Cameroon Volcanic Line (CVL), in Equatorial West Africa, along which both oceanic and continental alkali basalts were erupted. The CVL is a 1600 km long chain of Cenozoic volcanic and sub-volcanic complexes that straddles the continent–ocean boundary and extends from the Gulf of Guinea to the interior of the African continent (Fig. 1). The oldest magmatism is represented by poorly studied plutonic ring complexes of 60–30 Ma (Cantagrel *et al.*, 1978). Volcanic activity (42 Ma to the present) ranges from basaltic to more evolved phonolitic or trachytic compositions.

Differences between the mean chemical and Sr–Nd isotopic compositions of the mainly alkali basalts of the two sectors are, at a first glance, negligible (Fitton & Dunlop, 1985; Halliday *et al.*, 1988). This similarity has been used to infer an asthenospheric mantle source for the CVL alkaline basalts (Fitton & Dunlop, 1985). Small Pb isotopic differences between basalts from the continental and oceanic sectors were interpreted in terms of different contributions from HIMU, DMM and EM mantle source components (Halliday *et al.*, 1990; Lee *et al.*, 1994*a*).

The initiation of the volcanism in the oceanic sector of the CVL displays a time-related NE–SW shift, and magmatism on a single volcanic island may persist for as much as 30 My (Lee *et al.*, 1994*a*). $^{40}Ar/^{39}Ar$ ages of silicic volcanic rocks from the continental sector (Marzoli *et al.*, 1999) suggest NE–SW migration of the volcanism from Mt Oku (25 Ma) to Mt Bambouto (18–16 Ma). However, this younging trend does not apply to the entire silicic volcanism of the continental CVL, nor to published ages of the plutonic ring complexes (K/Ar ages: Cantagrel *et al.*, 1978). In general, the volcanism along the CVL cannot be interpreted as a single hotspot track, but may be the result of a linear mantle upwelling zone, or hotline, extending from NE to SW (Lee *et al.*, 1994*a*; Meyers *et al.*, 1998).

Whatever the origin of the CVL basaltic volcanism, the common signature of continental and oceanic basalts points to a similar sublithospheric mantle source. Here we present new $^{40}Ar/^{39}Ar$, major and trace element, and Sr–Nd isotopic data for three CVL continental volcanic complexes that show marked intra- and inter-volcanic differences in trace element concentrations and moderate differences in Sr isotopic composition. These differences suggest that a continental lithospheric signature overprinted the common asthenospheric signature of the CVL.

GEOLOGICAL SETTING

The crystalline basement of the CVL forms part of a mobile belt between the West Africa and Congo cratons (Fig. 1), and comprises Pan-African granitic rocks (Lassere, 1978) that yield Middle Proterozoic Nd model ages (Toteau *et al.*, 1994; W. R. Van Schmus, personal communication, 1994). These Pan-African granitoids are crossed by a major, still active fault belt, the Central African Shear Zone, that follows old Pan-African lineaments (Browne & Fairhead, 1983; Moreau *et al.*, 1987; Wilson & Guiraud, 1992) and has its counterpart in the NE Brazil Pernambuco lineament.

The Y-shape of the CVL (Fitton, 1987) mirrors the shape of the adjacent Mesozoic sedimentary basin of the Benue Trough, in which volumetrically scarce alkaline and tholeiitic magmatism, younging from north to south, occurred between 147 and 49 Ma (Maluski *et al.*, 1995). The alkali basalts of the Benue Trough are geochemically and isotopically similar to those of the CVL (Coulon *et al.*, 1996).

This study focuses on the magmatic activity of Mts Bambouto and Oku (Western Cameroon Highlands) and of the Ngaoundere Plateau (Fig. 1). These regions were uplifted, probably in the early Cenozoic shortly before the onset of the CVL magmatism (Browne & Fairhead, 1983). A regional negative Bouguer anomaly characterizes the volcanic highlands, particularly the Ngaoundere Plateau, where it reaches −120 mGal (Fairhead & Okereke, 1987). Seismic and gravity data suggest a general crustal thickness of ~30–34 km along the CVL continental sector with a lithospheric thickness of ~120–150 km, except in the Ngaoundere Plateau, where the crust and lithosphere are thinned to about 20–23 km and 80–100 km, respectively (Fairhead & Okereke, 1987;

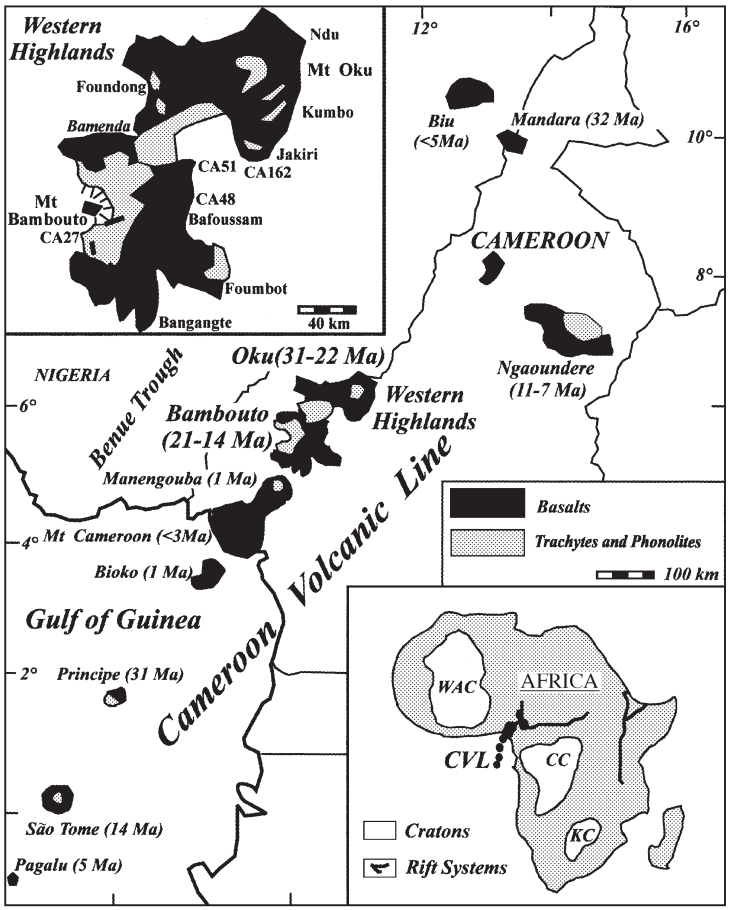

Fig. 1. Sketch map of the Cameroon Volcanic Line (CVL). Reported ages refer to the stratoid volcanism of the continental sector (Gouhier *et al.*, 1974; Fitton & Dunlop, 1985; Njilah, 1991; this study), and to the onset of the basaltic volcanism on the oceanic islands (Lee *et al.*, 1994*a*). Inset, top left: sketch map of Western Cameroon Highlands; Mt Bambouto caldera is shown, as well as location of basaltic samples used for $^{40}Ar/^{39}Ar$ dating. Inset, bottom right: the cratons are West African Craton (WAC), Congo Craton (CC) and Kalahari Craton (KC).

Plomerova *et al.*, 1993; Poudjom Djomani *et al.*, 1995, 1997).

Although paralleled in the north by the extensional structure of the Benue Trough, the relationship between regional tectonics and the CVL magmatism is still debated (Moreau *et al.*, 1987; Halliday *et al.*, 1988; Déruelle *et al.*, 1991). Only the volcanism of the Ngaoundere Plateau is clearly associated with the extensional tectonics responsible for the Adamawa horst and the Djerem and Mbere grabens. The whole CVL continental sector instead seems to follow an old suture zone between two seismically and palaeomagnetically distinct lithospheric blocks (Fairhead & Binks, 1991; Smith & Livermore, 1991; Plomerova *et al.*, 1993; Poudjom Djomani *et al.*, 1995).

Sampling and stratigraphy

A total of 130 basic rocks were sampled from the Mt Bambouto (55 samples), Mt Oku (53 samples) and Ngaoundere Plateau (22 samples) volcanic complexes (Fig. 1). Mt Bambouto [2700 m a.s.l. (above sea level)] and Mt Oku (3000 m a.s.l.) are Oligocene to Quaternary stratovolcanoes characterized by large collapse calderas, particularly well preserved at Mt Bambouto. The Mt Bambouto complex is characterized by five magmatic events: (1) extrusion of voluminous early stratoid basalt lava flow sequences (up to 600 m thick), which represent the peak of basaltic magmatism; (2) eruption, shortly before caldera formation, of trachytic lava flows and minor rhyolitic ignimbrites (Marzoli *et al.*, 1999); (3) intrusion of postcaldera basalt dykes into the trachytic flows, and volumetrically scarce basalt flows; and, finally, (5) a few pyroclastic and phreatomagmatic events representing the most recent volcanic activity.

For this study, basic lava flows and dykes of the precaldera and postcaldera to Quaternary magmatic events were collected from the volcanic plains south, east and north of the main volcanic edifice of Mt Bambouto. Single basaltic flow units reach a thickness of >50 m,

and the thickness of the sampled dykes varies from a few metres to ~30 m. Quaternary basalts were collected close to the town of Foumbot, ~50 km east of Mt Bambouto.

Field observations indicate for Mt Oku a succession of magmatic events similar to that of Mt Bambouto (see Njilah, 1991). Thick basalt lava sequences extend all around the main edifice and generally underlie silicic flows. Three ~400–600 m thick volcanic sequences were sampled in detail at Kumbo, Jakiri and Foundong, i.e. east, south and north of the main edifice, respectively.

The general stratigraphy of the volcanic Ngaoundere Plateau is similar to that of the Mt Bambouto and Mt Oku regions, with stratoid basalt flows underlying the Miocene volcanics of Mt Tchabal Nghana stratovolcano (~50 km east of Ngaoundere town), which is mainly composed of trachytic lava flows (Nono *et al.*, 1994). Minor basaltic flows and pyroclastic deposits were erupted in Quaternary times. Miocene to Quaternary basaltic rocks were collected on the Ngaoundere Plateau, to the east and north of the Ngaoundere town, i.e. on the southern and western slopes of Mt Tchabal Nghana stratovolcano.

$^{40}Ar/^{39}Ar$ AGES

Present (Fig. 2, Table 1) and previous $^{40}Ar/^{39}Ar$ (Lee *et al.*, 1994*b*; Marzoli *et al.*, 1999) and K/Ar data (Fitton & Dunlop, 1985) indicate that the oldest magmatic activity in the Mt Bambouto region is represented by scarce quartz-normative mugearites of the Bangangte area (e.g. CA74, Table 2) dated at 42 Ma (Lee *et al.*, 1994*b*; D. C. Lee, personal communication, 1995). However, the peak magmatic activity at Mt Bambouto is represented by slightly alkaline to subalkaline stratoid basaltic flows erupted between 21 Ma (sample CA51, $^{40}Ar/^{39}Ar$ plateau age of 20·8 ± 0·1 Ma) and 14 Ma (K/Ar; Fitton & Dunlop, 1985). The precaldera quartz trachyte lava flows and ignimbrites of the Bambouto main edifice range in age from 17·8 Ma to 15·5 Ma ($^{40}Ar/^{39}Ar$; Marzoli *et al.*, 1999; A. Marzoli, unpublished data, 1999). After caldera formation, basalt dykes (sample CA27, $^{40}Ar/^{39}Ar$ plateau age of 15·1 ± 0·1 Ma) intruded the silicic flows of the main edifice, and basanitic flows erupted in the caldera. Younger volcanic activity is mainly represented by basanitic and interlayered alkali basalt flows occurring on the eastern slopes of Mt Bambouto (CA48, $^{40}Ar/^{39}Ar$ plateau age of 4·5 ± 0·3 Ma).

The stratoid basalt volcanism of Mt Oku commenced in the northeastern regions (~31–23 Ma, Ndu area) and moved then to the SW (25–15 Ma, Bamenda area; Fitton & Dunlop, 1985; Njilah, 1991). A mugearite sample (CA162) belonging to the Jakiri basalt sequence, south of Mt Oku, yielded a $^{40}Ar/^{39}Ar$ plateau age of 23·4 ± 0·5 Ma. Finally, $^{40}Ar/^{39}Ar$ (Marzoli *et al.*, 1999) and K/Ar ages (Gouhier *et al.*, 1974) of Ngaoundere trachytes range between 11 and 7 Ma. Sporadic volcanism continued until the Quaternary in the Mt Bambouto, Mt Oku and Ngaoundere Plateau complexes.

ANALYTICAL METHODS

Major and trace elements (Table 2) of 130 samples were determined at the Dipartimento di Scienze della Terra, Trieste, Italy, using a PW 1404 XRF spectrometer and the procedures of Philips (1994) for the correction of matrix effects. The analytical uncertainties are less than 5% and 10% for major and trace elements, respectively. FeO was measured by titration and loss on ignition (LOI), corrected for FeO oxidation, by gravimetry. Rare earth elements (REE, 35 samples) were determined by inductively coupled plasma-mass spectrometry (ICP-MS) at the Centre de Recherches Pétrographiques et Géochimiques, CNRS, Vandoeuvre, France (Govindaraju & Mevelle, 1987). Representative analyses are given in Table 2. The complete dataset may be downloaded from the *Journal of Petrology* website at http://www.petrology.oupjournals.org. Mineral compositions of 22 selected samples were obtained with a CAMECA-CAMEBAX electron-microprobe operating at 15 kV and 15 nA, at the Dipartimento di Mineralogia e Petrologia, Padua, Italy. A PAP CAMECA program was used to convert X-ray counts into weight percent of the corresponding oxides. Results are considered accurate to within 2–3% for major and 10% for minor elements. Representative compositions are reported in Table 3.

Samples for Sr (35 samples) and Nd (18 samples) isotopic analysis were first dissolved in HF, HNO_3 and HCl in Teflon vials, followed by Sr and Nd collection by ion exchange and reversed-phase chromatography, respectively. The isotopic compositions were measured using a Finnigan MAT 262-RPQ mass spectrometer at the Centro di Studio per il Quaternario e l'Evoluzione Ambientale, CNR, Rome, Italy. Repeat analyses of NBS 987 and La Jolla standards gave average values of 0·71226(2) and 0·511857(8), respectively. No corrections were applied to the measured ratios for instrumental bias. The reported uncertainties on the Sr–Nd isotopic compositions are at the 2σ confidence level. Some samples were reanalysed after HCl (6 N) leaching, to test the possible effects of alteration. The analyses yielded Sr and Nd isotopic compositions coincident with those of the unleached samples, within analytical errors [0·70365(2) vs 0·70366(1), and 0·512874 (2) vs 0·512874 (2), respectively].

Approximately 5–10 mg of plagioclase mineral separates were used to determine $^{40}Ar/^{39}Ar$ crystallization

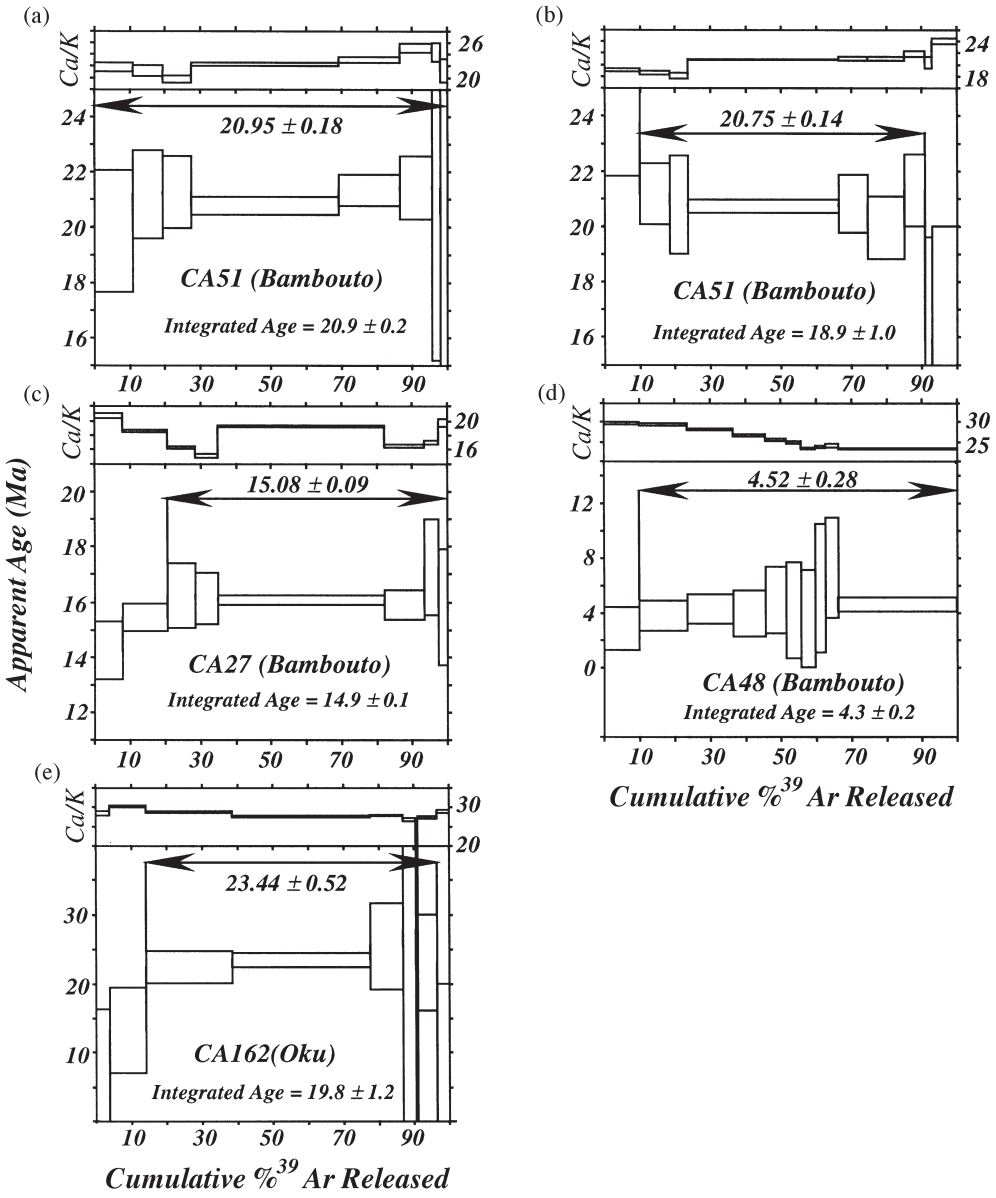

Fig. 2. $^{40}Ar/^{39}Ar$ step heating apparent age spectra for samples from Mt Bambouto and Mt Oku. (a) and (b) refer to two different analyses of sample CA51. Arrows show plateau steps. Errors are at the 2σ level, and include uncertainties in J values.

ages at the Berkeley Geochronology Center, USA. Plagioclase crystals were carefully hand picked to avoid altered or inclusion-bearing crystals and were irradiated for 7 h in the Triga reactor at Oregon State University, along with Fish Canyon sanidine (FCs) neutron fluence monitors. Plagioclase separates were step heated using a defocused NdYAG or Ar-ion laser beam. Ar isotopic compositions were measured in static mode by a MAP215-50 spectrometer, adopting procedures described by Renne (1995). Apparent ages were calculated assuming an age of 28·02 Ma for the FCs neutron fluence monitor (Renne *et al.*, 1998). Age uncertainties are given at the 2σ level, and do not reflect systematic errors in the age of the standard or the ^{40}K decay constants. All the analysed samples yielded plateaux (Fig. 2), defined by 6–9 contiguous steps and by 80–100% of cumulative ^{39}Ar released. Calculated Ca/K ratios (12–23) are homogeneous for each sample and consistent with measured mineral compositions (Table 3c), suggesting that the analysed mineral separates were composed of fresh and compositionally homogeneous plagioclases. One sample, CA51, was

Table 1: Ar/Ar data for basaltic samples from Mt Oku (CA162) and from Mt Bambouto (CA51, CA27, and CA48)

^{40}Ar (mol)	^{40}Ar/^{39}Ar	^{38}Ar/^{39}Ar	^{37}Ar/^{39}Ar	^{36}Ar/^{39}Ar	^{40}Ar*/^{39}Ar	% ^{40}Ar*	Age (Ma)	±2σ (Ma)
CA27 (Mt Bambouto, dyke)								
3·14E–15	15·48203	1·76E–02	9·562260	3·54E–02	5·811693	37·3	13·239	0·523599
2·72E–15	8·256433	1·27E–02	8·492586	8·87E–03	6·346290	76·5	14·453	0·2546421
1·52E–15	7·558524	1·33E–02	7·310306	5·01E–03	6·692292	88·1	15·237	0·5866535
1·26E–15	7·691748	0·0146064	6·730286	5·45E–03	6·645496	86·0	15·131	0·473571
9·57E–15	7·837849	1·32E–02	8·795094	6·61E–03	6·624010	84·0	15·083	9·20E–02
2·02E–15	7·144197	1·25E–02	7·396279	4·12E–03	6·548843	91·2	14·912	0·2656558
7·58E–16	7·437777	1·21E–02	7·646305	3·17E–03	7·146403	95·6	16·267	0·8703974
4·57E–16	6·835286	1·04E–02	9·055474	3·67E–03	6·510397	94·7	14·825	1·0525050
CA51 (Mt Bambouto, flow)								
6·96E–15	42·23605	2·85E–02	11·16898	0·1165992	8·735830	20·5	19·865	1·102360
2·71E–15	21·22344	1·58E–02	11·02138	4·35E–02	9·325030	43·6	21·197	0·7973481
1·93E–15	15·63172	1·57E–02	10·66807	2·43E–02	9·353935	59·4	21·262	0·6549639
8·75E–15	13·82672	1·44E–02	11·31214	1·92E–02	9·133152	65·6	20·763	0·1693812
2·79E–15	10·66742	1·11E–02	11·49400	7·65E–03	9·393596	87·4	21·352	0·2886012
1·45E–15	10·70394	1·04E–02	12·01922	7·80E–03	9·431410	87·4	21·437	0·5702517
4·10E–16	10·85413	−6·55E–03	11·84989	8·31E–03	9·416907	86·1	21·404	3·116538
3·33E–16	9·515896	5·86E–04	11·03346	4·89E–03	9·017365	94·1	20·501	3·286514
4·69E–15	23·41370	1·90E–02	9·766192	4·67E–02	10·45942	44·4	23·759	0·9680708
1·94E–15	11·54430	1·45E–02	9·49163	1·03E–02	9·323159	80·3	21·193	0·5585846
1·47E–15	14·21815	1·77E–02	9·31612	1·99E–02	9·148792	64·0	20·798	0·893683
8·73E–15	10·26581	1·27E–02	10·67892	6·96E–03	9·124306	88·3	20·743	0·1236992
1·57E–15	9·875748	1·06E–02	10·76598	5·52E–03	9·166615	92·2	20·839	0·5274043
1·95E–15	9·744165	1·19E–02	10·76284	6·38E–03	8·779680	89·5	19·964	0·5701268
1·19E–15	9·618103	8·57E–03	11·19299	4·08E–03	9·374981	96·8	21·310	0·6485025
4·30E–16	9·489779	9·69E–03	10·41697	0·0114554	6·983033	73·1	15·897	1·862847
CA162 (Mt Oku, flow)								
9·73E–14	586·9617	0·3968792	11·97774	2·015449	−7·709476	−1·3	−17·715	17·00266
9·39E–14	220·098	0·1490026	12·90907	0·7288083	5·814241	2·6	13·246	3·116841
1·24E–13	122·0303	8·38E–02	12·13696	0·3829932	9·902958	8·0	22·502	1·143988
1·07E–13	65·01299	4·69E–02	11·58122	0·1883395	10·36129	15·8	23·53	0·505866
9·63E–14	236·6902	0·1569025	11·73754	0·7664522	11·22643	4·7	25·489	3·137983
9·30E–14	635·5574	0·4041374	11·14368	2·112602	12·26197	1·9	27·821	18·44906
1·09E–14	351·0504	0·2316915	8·147403	1·156102	10·12569	2·9	23·006	32·39298
3·93E–14	169·3606	0·1129026	11·41821	0·5420519	10·17131	6·0	23·109	3·463513
7·09E–14	501·0684	0·3327219	12·26327	1·712008	−3·883695	−0·8	−8·902	14·45925

Age uncertainties are given at the 2σ level.

analysed twice, and yielded two indistinguishable plateau ages (20·95 ± 0·18 Ma, and 20·75 ± 0·14 Ma; Fig. 2a and b) from which the weighted mean of 20·83 ± 0·11 is adopted herein. Ar/Ar analytical data are reported in Table 1.

CLASSIFICATION

The classification of the basaltic flows and dykes was based on the total alkali–silica diagram (TAS; Le Bas *et al.*, 1986; Fig. 3; Table 2). Three main magmatic suites

Table 2: Major (wt %), trace element (ppm), normative, and measured (Sr_m and Nd_m) and initial isotopic (Sr_i and Nd_i) compositions of representative basaltic rocks from Mt Bambouto (Bamb), Mt Oku and Ngaoundere (Nga)

Sample:	CA54	CA 49	CA33	CA40	CA68	CA25	CA3	CA27	CA48
Type:	Bsn	Bsn	Teph	AkB	AkB	AkB	Haw	Haw	Haw
Area:	Bamb	Bamb	Bamb	Bamb	Bamb	Bamb	Bamb	Bamb	Bamb
SiO_2	42·38	42·97	44·69	47·32	46·71	46·30	47·16	48·02	49·25
TiO_2	4·24	4·75	3·81	2·87	4·03	3·32	2·99	3·01	2·93
Al_2O_3	12·79	14·07	14·52	15·27	16·78	15·93	15·36	16·05	17·88
FeO_t	12·30	12·62	11·96	11·28	10·82	11·05	10·92	10·55	10·03
MnO	0·19	0·18	0·22	0·18	0·17	0·19	0·18	0·20	0·21
MgO	11·54	9·47	7·18	7·53	5·85	5·61	7·25	6·06	3·66
CaO	11·63	10·83	10·54	10·39	9·86	12·51	9·94	9·78	9·21
Na_2O	2·69	3·47	3·88	3·48	3·09	2·58	3·62	3·66	3·79
K_2O	1·30	0·74	2·37	1·19	1·89	1·68	1·47	1·69	1·86
P_2O_5	0·94	0·90	0·83	0·49	0·80	0·83	1·11	0·98	1·18
FeO	9·85	10·14	10·77	8·66	9·55	9·43	8·84	8·28	7·56
Fe_2O_3	2·72	2·76	1·32	2·91	1·41	1·80	2·31	2·52	2·74
LOI	2·18	2·14	3·46	1·43	2·21	2·56	1·65	1·68	2·56
Cr	356	225	313	338	119	169	224	20	1
Ni	183	86	132	189	65	80	123	85	13
Ba	655	821	649	387	409	660	756	75	600
Rb	32	21	68	32	47	41	34	37	45
Sr	1643	1963	1355	610	992	1525	1206	1344	1608
Zr	151	81	366	243	319	167	171	220	255
Y	34	32	40	33	43	37	36	36	45
Nb	71	64	117	59	87	77	61	69	97
La	49·85	41·27	64·44	37·35	53·72	48·16	43*	48*	61·05
Ce	105·49	90·26	122·28	76·25	112·73	97·49	83*	94*	122·60
Nd	57·21	51·66	54·74	37·95	57·03	48·81	46·12	52·31	59·02
Sm	11·99	11·24	10·65	8·16	11·30	10·39	10·25	11·05	11·50
Eu	3·91	3·78	3·24	2·52	3·33	3·19			3·51
Gd	8·78	8·12	8·27	6·70	8·73	7·95			8·86
Dy	5·87	5·54	6·08	5·44	6·70	5·96			6·63
Er	2·47	2·26	2·76	2·47	2·91	2·56			3·04
Yb	2·01	1·87	2·49	2·05	2·44	2·18			2·53
Lu	0·26	0·24	0·36	0·30	0·38	0·30			0·36
$(La/Yb)_{cn}$	16·72	14·88	17·45	12·28	14·84	14·89			16·27
mg-no.	0·66	0·61	0·55	0·58	0·53	0·51	0·58	0·54	0·43
Q									
Ne	9·63	8·62	13·88	4·62	2·35	2·21	4·04	3·61	1·87
Ol/Hy									
$(Sr)_m$	0·70357(3)	0·70367(2)	0·70355(3)	0·70312(3)	0·70322(1)	0·70343(2)	0·70342(3)	0·70343(1)	0·70332(2)
$(Nd)_m$		0·512852(1)	0·512857(3)	0·512855(3)		0·512917(7)	0·512856(5)	0·512853(2)	
$(Sr)_i$	0·70356	0·70365	0·70354	0·70313	0·70321	0·70342	0·70341	0·70342	0·70332
$(Nd)_i$		0·512854	0·512858	0·512856		0·512918	0·512857	0·512855	
Age (Ma)	15	15	15	21	21	15	15	15	5

Table 2: continued

Sample:	CA38	CA13	CA 51	CA4	CA50	CA74	CA165	CA166	CA163	CA167
Type:	Haw	Mug	Mug	TrB	TrB	Mug	AkB	TrB	TrB	TrB
Area:	Bamb	Bamb	Bamb	Bamb	Bamb	Bamb	Oku	Oku	Oku	Oku
SiO_2	48·97	52·94	52·64	48·88	49·51	54·61	45·92	46·73	47·43	46·75
TiO_2	2·95	1·84	2·20	2·63	2·95	2·60	3·41	3·44	3·93	4·25
Al_2O_3	18·14	16·49	17·61	15·15	16·42	14·32	15·31	14·97	16·50	16·77
FeO_t	11·19	11·87	9·64	10·51	10·45	13·05	11·22	11·43	11·87	12·64
MnO	0·20	0·21	0·20	0·19	0·17	0·19	0·18	0·19	0·17	0·25
MgO	3·58	2·27	2·69	8·06	5·49	2·27	8·07	9·41	6·63	6·48
CaO	8·18	5·91	7·12	8·75	9·44	6·52	10·69	9·12	8·66	8·34
Na_2O	4·32	4·42	4·35	3·39	3·14	3·69	3·01	2·60	3·07	2·79
K_2O	1·74	2·44	2·58	1·33	1·74	1·64	1·47	1·34	1·16	1·04
P_2O_5	0·73	1·61	0·97	1·11	0·69	1·11	0·72	0·77	0·58	0·69
FeO	8·93	9·85	7·31	7·90	7·44	9·66	9·56	9·22	9·27	9·64
Fe_2O_3	2·51	2·24	2·59	2·90	3·34	3·77	1·84	2·46	2·89	3·33
LOI	1·19	2·13	4·09	2·45	2·12	2·43	2·07	2·96	1·94	2·79
Cr	19	5	17	256	152	1	426	200	132	35
Ni	25	13	24	168	73	7	180	106	62	33
Ba	547	1029	1144	825	798	563	486	484	398	354
Rb	33	36	50	36	38	35	32	27	24	21
Sr	906	809	1093	1308	1015	400	1034	813	903	791
Zr	279	455	348	179	195	335	195	236	227	203
Y	40	58	44	33	33	64	29	30	30	27
Nb	76	89	86	59	59	39	62	67	60	55
La	47·66	78·55	75*	42·62	40·49	38·64	37·79	41·76	38·35	33·65
Ce	97·65	168·96	149*	86·98	82·61	86·03	78·44	88·73	80·99	72·95
Nd	48·06	86·43	73*	43·41	40·53	50·06	41·24	45·05	43·18	38·74
Sm	10·20	17·21		9·01	8·62	12·60	8·43	8·95	8·86	8·03
Eu	3·21	4·92		3·08	2·66	3·73	2·93	3·09	2·91	2·64
Gd	7·94	13·12		6·95	7·01	11·02	6·90	7·56	7·32	6·22
Dy	6·59	9·83		5·11	5·54	9·60	5·15	5·47	5·58	4·54
Er	2·87	4·32		2·23	2·56	4·42	2·28	2·39	2·32	2·02
Yb	2·51	3·94		1·89	2·21	3·82	1·83	1·91	1·93	1·64
Lu	0·36	0·55		0·28	0·31	0·54	0·28	0·30	0·29	0·27
$(La/Yb)_{cn}$	12·80	13·44		15·20	12·35	6·82	13·92	14·74	13·40	13·83
mg-no.	0·40	0·28	0·366	0·61	0·52	0·27	0·60	0·63	0·54	0·52
Q						7·41				
Ne	2·91						4·76			
Ol/Hy		0·01	0·12	2·99	1·12			4·46	1·62	0·59
$(Sr)_m$	0·70326(2)	0·70509(2)		0·70352(3)		0·70512(2)	0·70357(1)	0·70336(1)	0·70337(5)	0·70383(1)
$(Nd)_m$	0·512854(5)	0·512496(3)		0·512836(2)			0·512616(8)		0·512846(2)	
$(Sr)_i$	0·70325	0·70507		0·70351		0·70515	0·70356	0·70335	0·70337(5)	0·70382
$(Nd)_i$	0·512854	0·512498		0·512836		0·512614		0·512846(2)		
Age (Ma)	21	15	21	15	21	42	23	23	23	23

Sample:	CA172	CA175	CA162	CA132	CA136	CA129	CA127	CA148	CA130	CA141
Type:	Mug	Mug	Mug	Bsn	Bsn	Teph	PTeph	AkB	AkB	AkB
Area:	Oku	Oku	Oku	Nga	Nga	Nga	Nga	Nga	Nga	Nga
SiO_2	53·20	55·41	52·24	41·93	43·91	45·74	46·87	45·27	45·28	48·10
TiO_2	2·25	1·73	2·26	3·35	3·17	2·79	2·62	3·73	2·56	2·62
Al_2O_3	16·75	16·33	16·99	12·80	13·90	14·49	15·47	13·09	13·74	15·74
FeO_t	10·75	10·00	11·98	13·77	11·03	10·48	10·81	12·14	10·71	9·67
MnO	0·22	0·20	0·26	0·21	0·19	0·12	0·24	0·17	0·19	·15
MgO	2·98	2·89	2·17	10·29	9·61	9·07	4·62	11·18	10·81	8·19
CaO	5·61	4·71	7·24	11·29	11·19	10·05	9·69	10·85	10·66	9·31
Na_2O	5·08	5·08	3·46	4·37	4·57	4·43	5·73	2·46	3·17	4·14
K_2O	2·15	2·39	2·27	1·31	1·56	2·01	3·06	0·60	1·84	1·41
P_2O_5	1·01	1·26	1·13	0·68	0·87	0·82	0·89	0·51	1·04	·66
FeO	7·25	6·36	8·98	10·18	7·59	8·17	7·69	9·66	8·48	7·37
Fe_2O_3	3·89	4·04	3·33	3·99	3·82	2·49	3·47	2·76	2·48	2·56
LOI	1·83	2·77	3·81	0·99	1·23	1·25	1·13	2·84	2·25	2·53
Cr	6	4	13	361	314	520	201	340	431	358
Ni	9	10	12	205	175	252	90	116	245	240
Ba	585	628	1063	515	598	715	823	356	722	648
Rb	39	34	62	39	42	54	73	24	50	43
Sr	939	793	861	1043	983	1007	1350	566	982	910
Zr	403	511	346	290	251	276	470	244	260	244
Y	47	50	46	35	34	32	41	29	35	26
Nb	92	102	76	102	114	113	141	62	111	95
La	60·86	73·11	66·49	67·67	70·28	63·78	98·33	33·85	68·03	55·14
Ce	127·80	150·70	142·00	131·10	131·10	119·50	177·20	71·99	124·70	99·43
Nd	65·34	73·48	71·01	59·80	58·25	51·82	69·02	37·67	52·74	43·31
Sm	12·81	13·93	13·63	11·32	10·86	10·04	11·53	8·08	9·49	8·07
Eu	4·04	4·13	4·07	3·26	3·33	3·08	3·43	2·56	2·92	2·59
Gd	10·61	11·59	10·82	8·88	8·98	8·09	9·40	7·10	7·87	6·41
Dy	7·48	8·17	7·78	6·43	6·05	5·53	6·72	5·22	5·54	4·43
Er	3·22	3·62	3·56	2·54	2·51	2·34	3·01	2·39	2·48	1·94
Yb	2·70	3·02	3·05	1·96	2·00	1·73	2·57	1·71	1·97	1·49
Lu	0·45	0·41	0·44	0·28	0·30	0·27	0·40	0·25	0·30	0·23
$(La/Yb)_{cn}$	15·20	16·32	14·70	23·28	23·69	24·86	25·80	13·35	23·28	25·12
mg-no.	0·37	0·37	0·27	0·61	0·64	0·64	0·27	0·66	0·68	0·64
Q		0·37	2·29							
Ne				20·03	18·84	15·24	22·26	1·48	9·23	19·98
Ol/Hy										1·28
$(Sr)_m$	0·70362(1)	0·70366(1)	0·70474(2)	0·70317(1)	0·70288(1)	0·70337(1)	0·70341(2)	0·70327(1)	0·70341(1)	0·70304(1)
$(Nd)_m$										
$(Sr)_i$	0·70361	0·70365	0·70472	0·70317	0·70288	0·70337	0·70341	0·70327	0·70341	0·70304
$(Nd)_i$										
Age (Ma)	23	23	23	<11	<11	<11	<11	<11	<11	<11

Ages used for calculations of initial isotopic ratios are either measured $^{40}Ar/^{39}Ar$ ages (see Fig. 2) or inferred approximately from stratigraphic relations. REE concentrations measured by ICP-MS, except *measured by XRF. LOI, loss on ignition; *mg*-number = $Mg/(Mg + Fe^{2+})$, with $Fe_2O_3/FeO = 0·18$; cn, chondrite-normalized (Boynton, 1984) ratio; Q, normative quartz; Ne, nepheline; Ol, olivine; Hy, hypersthene. Bsn, basanite; Teph, tephrite; AkB, alkali basalt; Haw, hawaiite; Mug, mugearite; TrB, transitional basalt; Pteph, phono-tephrite.

Table 3: Representative phenocryst core (Phc) and groundmass (Gr) compositions of olivine (a), clinopyroxene (b), plagioclase (c), and opaque minerals (d) in basaltic rocks

(a) Olivine

Sample:	CA54	CA54	CA33	CA33	CA25	CA25	CA75	CA75	CA51	CA50	CA50	CA165	CA165	CA166	CA129	CA129	CA128	CA128	CA130	CA130	CA148	CA148	CA133	CA133
Type:	Phc	Gr	Phc	Gr	Phc	Gr	Phc	Gr	Gr	Phc	Gr	Phc	Gr	Phc	Phc	Gr	Phc	Gr	Phc	Gr	Phc	Gr	Phc	Gr
Area:	Bamb	Bamb	Bamb	Bamb	Bamb	Bamb	Bamb	Bamb	Bamb	Bamb.	Bamb.	Oku	Oku	Oku	Nga	Nga	Nga	Nga	Nga	Nga	Nga	Nga	Nga	Nga
Rock type:	Bsn	Bsn	Teph	Teph	AkB	AkB	Haw	Haw	Mug	TrB	TrB	AkB	AkB	TrB	Teph	Teph	Pteph	Pteph	AkB	AkB	AkB	AkB	Haw	Haw
SiO_2	40·14	37·59	39·45	38·91	38·92	36·03	38·24	37·12	36·84	39·52	38·27	39·30	37·82	38·37	40·57	40·39	39·60	38·89	40·40	38·57	38·82	38·34	39·66	38·32
Al_2O_3	0·00	0·03	0·02	0·00	0·01	0·00	0·03	0·00	0·01	0·01	0·00	0·16	0·00	0·00	0·00	0·00	0·00	0·00	0·00	0·01	0·05	0·02	0·03	0·04
FeO_t	12·96	24·63	16·32	16·20	18·93	34·27	22·67	28·06	30·35	16·89	23·14	15·36	25·06	21·11	11·70	12·71	15·42	17·87	10·13	19·95	19·44	21·23	14·47	23·09
MnO	0·18	0·49	0·18	0·25	0·37	0·78	0·33	0·62	0·81	0·27	0·45	0·19	0·54	0·32	0·15	0·22	0·27	0·32	0·15	0·39	0·35	0·31	0·16	0·53
MgO	46·10	35·90	43·28	42·55	41·31	28·04	38·39	33·43	31·48	42·69	37·76	44·06	36·21	39·80	47·53	46·69	44·12	42·01	48·74	39·99	40·85	38·43	45·56	37·57
CaO	0·30	0·56	0·25	0·32	0·33	0·64	0·26	0·31	0·19	0·27	0·25	0·30	0·37	0·26	0·05	0·05	0·29	0·28	0·15	0·41	0·28	0·26	0·17	0·34
Sum	99·68	99·20	99·50	98·23	99·87	99·76	99·92	99·54	99·68	99·65	99·87	99·37	100·00	99·86	100·00	100·06	99·70	99·37	99·57	99·32	99·79	99·59	100·06	99·89
Fo	86·13	71·22	82·06	81·81	78·86	58·22	74·58	67·20	64·07	81·31	73·78	83·14	71·25	76·26	87·68	86·51	82·99	80·14	89·23	77·37	78·30	76·24	84·53	73·53
Fa	13·57	27·43	17·38	17·49	20·28	39·92	24·73	31·65	34·67	18·04	25·36	16·26	27·65	23·03	12·12	13·19	16·31	19·11	10·42	21·68	20·90	23·07	15·07	25·36
Tph	0·20	0·55	0·20	0·27	0·40	0·90	0·34	0·70	0·95	0·30	0·50	0·20	0·60	0·36	0·15	0·25	0·30	0·35	0·15	0·40	0·40	0·35	0·15	0·61
Lar	0·10	0·80	0·36	0·46	0·45	0·96	0·35	0·45	0·31	0·35	0·36	0·40	0·50	0·35	0·05	0·05	0·40	0·40	0·20	0·55	0·40	0·34	0·25	0·50

Fo, forsterite; Fa, fayalite; Tph, tephroite; Lar, larnite.

(b) Clinopyroxene

Sample:	CA54	CA54	CA33	CA33	CA25	CA25	CA75	CA75	CA50	CA50	CA165	CA165	CA166	CA166	CA130	CA129	CA129	CA128	CA128	CA148	CA148	CA141	CA133	CA133
Type:	Phc	Gr	Phc	Gr	Phc	Gr	Phc	Gr	Mcc	Phc	Phc	Gr	Phc	Gr	Gr	Phc	Gr	Phc	Gr	Mcc	Phc	Phc	Phc	Gr
Area:	Bamb	Bamb	Bamb	Bamb	Bamb	Bamb	Bamb	Bamb	Bamb	Bamb	Oku	Oku	Oku	Oku	Nga	Nga	Nga	Nga	Nga	Nga	Nga	Nga	Nga	Nga
Rock type:	Bsn	Bsn	Teph	Teph	AkB	AkB	Haw	Haw	TrB	TrB	AkB	AkB	TrB	TrB	AkB	Teph	Teph	Pteph	Pteph	AkB	AkB	AkB	Haw	Haw
SiO_2	44·41	45·81	46·16	44·04	48·05	46·90	48·85	44·17	46·74	48·67	48·64	47·10	48·56	47·39	47·25	43·18	42·26	50·60	45·99	47·22	48·45	43·98	46·93	44·81
TiO_2	4·35	3·77	2·94	4·61	2·14	2·43	1·68	3·43	2·43	1·96	2·30	3·50	2·09	2·48	2·61	4·39	5·04	1·21	3·42	2·85	2·09	4·24	2·46	4·07
Al_2O_3	8·25	6·38	8·34	8·75	5·51	6·57	4·68	8·77	9·10	5·82	5·43	6·29	5·01	6·74	5·57	9·02	10·32	3·74	6·95	7·77	6·38	8·90	9·04	8·32
FeO_t	6·74	7·56	6·40	7·37	7·58	6·71	8·53	9·64	7·28	7·68	6·55	7·90	7·97	7·04	7·63	8·43	8·49	6·00	8·16	6·95	6·84	7·05	7·92	7·87
MnO	0·15	0·12	0·06	0·08	0·18	0·05	0·30	0·17	0·12	0·14	0·10	0·17	0·22	0·09	0·11	0·12	0·05	0·05	0·23	0·07	0·19	0·09	0·13	0·16
MgO	11·47	12·45	12·25	11·02	12·92	12·89	14·00	10·74	11·02	12·76	13·62	12·71	13·45	13·12	12·44	11·14	10·18	14·95	11·76	12·69	13·36	11·69	12·82	11·52
CaO	22·98	23·29	22·69	22·87	22·03	22·56	20·23	21·46	22·58	21·48	22·34	22·02	21·95	22·36	22·97	23·30	23·26	22·25	22·84	21·63	21·82	22·57	19·35	22·47
Na_2O	0·88	0·60	0·71	0·60	0·63	0·55	0·77	0·62	0·51	0·60	0·37	0·30	0·54	0·51	0·61	0·54	0·54	0·67	0·57	0·75	0·70	0·50	0·87	0·49
Cr_2O_3	0·00	0·04	0·00	0·01	0·05	0·52	0·15	0·00	0·04	0·08	0·17	0·07	0·01	0·24	0·01	0·02	0·03	0·35	0·05	0·02	0·19	0·75	0·02	0·25
Sum	99·23	100·02	99·55	99·35	99·09	99·18	99·19	99·00	99·82	99·19	99·52	100·06	99·80	99·97	99·20	100·14	100·17	99·82	99·97	99·96	100·02	99·77	99·54	99·96
Fe_2O_3	4·27	3·96	3·12	2·62	2·84	3·25	3·72	3·80	0·27	1·55	1·14	0·93	3·15	2·93	3·65	5·86	4·38	2·96	3·56	2·01	2·44	3·13	1·56	2·64
Ca	51·84	49·87	50·67	51·95	47·83	49·32	43·40	48·74	51·66	47·42	48·09	47·88	46·64	48·42	49·60	51·24	52·72	46·57	49·94	48·34	47·55	50·82	44·48	52·22
Mg	35·97	37·16	38·06	34·83	39·02	39·17	41·79	33·93	35·07	39·16	40·75	38·42	39·77	39·53	37·40	34·08	32·11	43·55	35·77	39·45	40·51	36·62	41·02	35·80
Fe*	12·18	12·18	11·27	13·22	13·15	11·51	14·81	17·33	13·27	13·42	11·16	13·70	13·59	12·05	13·00	14·68	15·15	9·88	14·29	12·21	11·94	15·56	14·50	13·98
Al^{VI}	0·031	0·000	0·083	0·048	0·044	0·043	0·029	0·067	0·146	0·080	0·049	0·037	0·026	0·052	0·019	0·016	0·044	0·027	0·030	0·089	0·069	0·040	0·138	0·046
T (°C)	1140	1041	1157	1259	1176	877	1103	1128		1287	1252	1146	1131	978	1130	1250	1322	1106			1139	1238	1333	1155
P (kbar)	1·05	0·00	3·59	0·40	0·26	1·08	0·99	1·54	4·55	1·64	0·10	0·00	0·00	1·38	0·00	0·00	0·36	0·46	0·00	3·91	2·64	1·26	7·96	0·36

Crystallization temperature (T) and pressure (P) are calculated according to Loucks (1996) and Nimis (1995), respectively. Fe* = FeO + Fe_2O_3 + MnO.

Table 3: continued

(c) Plagioclase

Sample:	CA54	CA33	CA25	CA51	CA51	CA50	CA50	CA50	CA74	CA74	CA166	CA166	CA165	CA162	CA162
Type:	Gr	Gr	Gr	Phc	Gr	Mcc	Phc	Gr	Phc	Gr	Phc	Gr	Gr	Phc	Gr
Area:	Bamb	Bamb	Bamb	Bamb	Bamb	Bamb	Bamb	Bamb	Bamb	Bamb	Oku	Oku	Oku	Oku	Oku
Rock type:	Bsn	Teph	AkB	Mug	Mug	TrB	TrB	TrB	Mug	Mug	AkB	AkB	AkB	Mug	Mug
SiO_2	49·57	52·35	51·78	54·40	54·86	60·82	54·59	51·13	53·51	56·85	47·45	56·67	55·79	53·93	55·90
TiO_2	0·24	0·19	0·19	0·08	0·16	0·05	0·08	0·13	0·15	0·12	0·11	0·21	0·17	0·05	0·11
Al_2O_3	31·53	29·87	30·32	28·71	27·93	24·24	28·60	30·56	29·13	26·83	33·37	26·15	27·41	29·07	27·43
FeO	1·02	0·54	0·55	0·37	0·68	0·24	0·40	0·84	0·60	0·58	0·54	0·86	0·59	0·38	0·53
CaO	14·45	12·42	12·94	10·99	10·26	5·81	10·86	13·26	11·54	8·86	16·46	8·35	9·60	11·40	9·60
Na_2O	3·08	4·15	3·98	5·02	5·36	7·45	5·09	3·71	4·81	6·17	2·05	4·99	5·44	4·76	5·56
K_2O	0·18	0·41	0·24	0·43	0·44	1·32	0·44	0·28	0·21	0·50	0·07	2·55	0·93	0·47	0·77
Sum	100·07	99·93	100·00	100·00	99·69	99·93	100·07	99·91	99·95	99·91	100·05	99·78	99·93	100·06	99·91
Or	1·08	2·41	1·39	2·56	2·63	7·80	2·64	1·66	1·28	3·00	0·41	15·27	5·55	2·81	4·60
Ab	26·38	35·42	35·29	42·68	45·90	63·25	43·28	31·78	40·99	52·66	17·49	42·75	46·45	40·44	47·44
An	72·54	61·87	63·33	54·76	51·48	28·95	54·08	66·56	57·73	44·34	82·10	41·98	48·00	56·75	47·96
T_h (°C)	1140	1100	1108	1032	1013	897	1025	1095	952	863	1180	976	1021	1022	976
T_d (°C)	1251	1221	1224	1176	1162	1061	1165	1217	1128	1069	1285	1128	1159	1168	1134

An, anorthite; Ab, albite; Or, orthoclase; feldspar crystallization dry and hydrous conditions temperatures (T_d and T_h, respectively) are calculated according to Mathez (1973). Other abbreviations as in Table 2.

(d) Opaque minerals

Sample:	CA25	CA130	CA150	CA150	CA150
Rock type:	AkB	AkB	TrB	TrB	TrB
Area:	Bamb	Nga	Nga	Nga	Nga
Oxide:	Mt	Mt	Mt	Ilm	Ilm
SiO_2	0·07	0·07	0·05	0·25	0·07
TiO_2	27·12	21·17	22·02	50·33	52·06
Al_2O_3	2·54	5·39	2·59	0·13	0·09
FeO_t	64·27	64·40	69·76	41·07	39·40
MnO	0·80	0·68	0·40	0·51	0·52
MgO	2·44	4·35	3·16	4·16	5·18
CaO	0·12	0·08	0·15	1·02	0·18
Cr_2O_3	0·16	1·75	0·12	0·04	0·00
Sum	97·52	97·89	98·25	97·51	97·50
Ulvöspinel					
FeO	51·75	44·36	46·84	36·32	36·91
Fe_2O_3	13·90	22·28	25·46	5·28	2·76
Sum	98·92	100·12	100·79	98·03	97·77
% Ulvösp.	76·54	59·33	60·97		
% R_2O_3				5·18	2·77
T (°C)				900	812
fO_2				13·25	15·75

can be distinguished: (1) basanite–tephrite–phonotephrite (BSN series; CIPW nepheline, Ne = 9–24%); (2) alkali basalt–Ne hawaiite–Ne mugearite (AKB series, Ne = 1–11%); (3) CIPW hypersthene, Hy basalt (named hereafter transitional basalts)–Hy hawaiite–Hy or quartz mugearite (TRB series; Hy = 1–23% or Q = 2–3%).

PETROGRAPHY AND MINERAL COMPOSITIONS

The investigated basaltic samples are petrographically fresh, do not contain secondary minerals and are mostly aphyric or slightly porphyritic. Samples with more than 10 vol. % phenocrysts are rare and mainly belong to the alkaline volcanics of the Ngaoundere Plateau. The most common phenocrysts (Table 3) are olivine and clinopyroxene, with subordinate magnetite and plagioclase. Olivine predominates over clinopyroxene phenocrysts in strongly alkaline samples (BSN suite), whereas the opposite occurs in the moderately alkaline and subalkaline samples (AKB and TRB suites). Plagioclase is a common phenocryst in the TRB suite samples and, less frequently (~5%), in Ne hawaiites and Ne mugearites. Apatite is present as small microphenocrysts in all the suites.

Olivine is commonly found as a phenocryst phase in most of the samples investigated, except Hy hawaiites

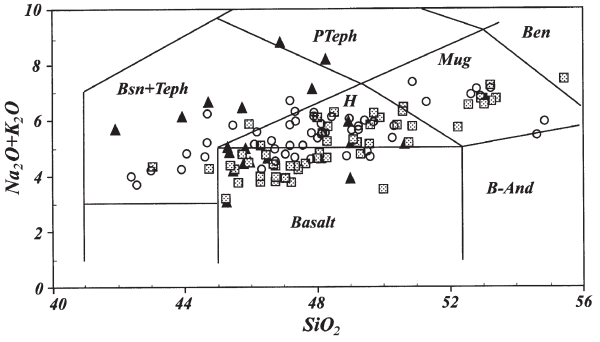

Fig. 3. Total alkali–silica (TAS) classification diagram (Le Bas *et al.*, 1986) of Mt Bambouto (○), Ngaoundere (▲) and Mt Oku samples (grey squares). Bsn, basanite; Teph, tephrite; PTeph, phono-tephrite; H, hawaiite; Mug, mugearite; Ben, benmoreite; B-And, basaltic andesite.

and mugearites, where it represents a groundmass phase. The porphyritic samples may have large resorbed and moderately altered olivine phenocrysts, whereas the subaphyric ones sometimes contain skeletal crystals indicating high crystallization temperature and high cooling rates. In general, the phenocryst cores have forsterite (Fo) ranging from 75 to 89% (mean 81 ± 4%), whereas the Fo content of the groundmass varies between 29 and 85% (mean 67 ± 13%; Table 3a). A systematic Fo decrease from early to late-crystallized olivines was observed for each sample.

The relationship between the Fo content of the phenocryst cores and the *mg*-number [Mg/(Mg + Fe^{2+})] of the bulk rocks suggests that olivines generally crystallized under low pressure and equilibrium conditions with a K_d (Fe^{2+}/Mg partition coefficient between olivine and melt) of 0·30–0·33 (Roeder & Emslie, 1970). However, several olivine compositions correspond to a K_d of ~0·25, suggesting that this may reflect a compositional effect and/or a relatively high fO_2 (e.g. Fe_2O_3/FeO ~0·25), owing to the alkaline nature of the investigated rocks.

Clinopyroxene (cpx) is generally represented by euhedral and weakly zoned pinkish phenocrysts in all the porphyritic samples, except the more evolved rocks (MgO < 3·0 wt %) where it is a groundmass phase. Some basanites may contain zoned cpx with a pink rim and a green core. Compositionally (Table 3b), cpx corresponds to salites and rarely to augites, which predominate in the more evolved samples. In terms of atomic Ca–Mg–Fe* (Fe* = Fe^{2+} + Mn + Fe^{3+}) relationships all cpx, including those of the transitional basalt suite, define phenocryst core to groundmass trends characterized by increasing Fe* and by constant or slightly increasing wollastonite component, consistent with the alkaline nature or affinity of the parental magmas.

Using the geobarometer of Nimis (1995), based on crystal-structure modelling, the pressure of cpx crystallization was estimated. The structural parameters were

calculated following the program of Ottonello *et al.* (1992), which allows simulation of the geometry of a C_2/c pyroxene from its chemical composition. An intracrystalline temperature of 1100°C was assumed for the distribution of Fe^{2+} and Mg between the M1 and M2 sites. The pressure was calculated only for the megacryst and phenocryst cores, as they better approach a near-liquidus crystallization (see Nimis, 1995). The relationships between the cell and M1 site volumes indicate for the phenocryst cpx a low pressure of crystallization (0–4·3 kbar; Table 3b), except for the cpx of the hawaiite CA133, which yielded a pressure of 8·0 kbar. The pressure of the megacrysts (e.g. CA148) ranges from 3·9 to 4·6 kbar and is similar to the highest one obtained for the phenocryst cpx.

The olivine–clinopyroxene Fe^{2+}–Mg exchange geothermometer of Loucks (1996) for early crystallized olivines and augites yielded temperatures ranging from 1250 ± 52 to 1106 ± 40°C (BSN suite), 1338 ± 54 to 1100 ± 43°C (AKB suite) and 1280 ± 35 to 1130 ± 63°C (TRB suite), respectively (Table 3b).

Plagioclase phenocrysts are commonly found in the rock types of the TRB suite and, sometimes, in those of the AKB suite. The anorthite (An) content (Table 3c) of the phenocryst core and groundmass plagioclases ranges from 82 to 42 wt %, but some transitional (e.g. CA50) and alkali (e.g. CA141) basalts may contain plagioclase megacrysts with relatively low An contents (e.g. 29–34 and 47–49 wt %, respectively), suggesting a xenocrystic origin. Finally, temperatures calculated according to Mathez (1973) for the early crystallized plagioclase phenocrysts range from 1289 to 1162°C for dry conditions and from 1180–1013°C for hydrous conditions (P_{H_2O} = 0·5 kbar). These temperatures, compared with those calculated for olivine–clinopyroxene pairs, suggest near-anhydrous conditions for plagioclase crystallization.

Opaque minerals (Table 3d) are mainly represented by magnetites with ulvöspinel content of 52–78%. The homogeneous groundmass magnetite–ilmenite pairs of the transitional basalt CA150 yielded $-\log fO_2$ of 13·25 and 15·75, and corresponding T values of 900 and 812°C [approximately the QFM (quartz–fayalite–magnetite) buffer].

In summary, from the mineral chemistry it appears that most early formed minerals, megacrysts included, crystallized within the crust, close to QFM buffer conditions and at low P_{H_2O}.

GEOCHEMISTRY

Major and trace elements

The variations of selected major and trace elements relative to MgO are shown in Fig. 4. In general, basanitic rock types predominate on the Ngaoundere Plateau, transitional basalts on Mt Oku, and alkali basalts on Mt Bambouto. Mt Bambouto volcanism tends to become more alkaline with time, similar to that of Mt Oku (Njilah, 1991). The Ngaoundere Plateau samples are characterized, at similar MgO content, by higher amounts of Nb (up to 140 ppm; Table 2) relative to samples from Mts Oku and Bambouto, which, instead, have higher FeO_t, Sr, Ba and P_2O_5 (Fig. 4).

Despite the general compositional similarity of the oceanic and continental CVL basalts (Fitton & Dunlop, 1985; Fig. 5), the minor and trace element concentrations in specimens from the continental sector exhibit a large range of variations (Table 2; Fig. 4). For example, primitive Mt Bambouto alkali basalts with almost identical major element compositions (compare CA40 and CA3, Table 2) have Sr concentrations that vary from 600 to 1300 ppm. Ba, P and Zr abundances display a similar variability. The ratios between Ba, Sr, P and Zr and other incompatible elements [e.g. light REE (LREE)] in the less evolved Mt Bambouto basalts (MgO > 6 wt %) reveal wide variations for similar (high) LREE concentrations (Fig. 6). These differences cannot be easily related to different degrees of fractional crystallization from a common parental magma (see Fig. 4), or to different degrees of partial melting of the same mantle source (see Fig. 6).

Samples with a mantle-normalized positive spike at Sr, relative to Ce and Nd (Fig. 5), are hereafter designated as high-Sr basalts (HSrB). Generally, HSrB are also characterized by strongly positive Ba and P spikes, and by negative Zr anomalies. In contrast, the basalts designated hereinafter as low in Sr (LSrB) are characterized by moderately negative or absent Sr and P anomalies, and by moderately positive Ba anomaly (Fig. 5).

There is a continuous compositional spectrum between HSrB and LSrB (Fig. 6). Approximately 35% of the Mt Bambouto basalt samples are of HSr type. These samples mainly belong to the BSN suite and represent the late magmatic events (15–4 Ma): dyke intrusions in the trachytic lava flows of the main edifice, intracaldera flows and postcaldera flows to the east of Mt Bamouto. The early (21–14 Ma) basaltic flows that cover the plains around Mt Bambouto are generally of LSr type and belong to the AKB and TRB suites. Only ~10% of Mt Oku basaltic volcanics are of HSr type (BSN and AKB suites), whereas HSrB are absent among those from the Ngaoundere Plateau. Notably, nephelinitic rocks from Mt Etinde, at the continent–ocean boundary on the SW slopes of Mt Cameroon, are characterized by extreme enrichments of Sr and Ba (up to 10 000 and 3000 ppm, respectively; Nkoumbo *et al.*, 1995), recalling HSr-type compositions. We emphasize that the compositional characteristics of HSrB have not been described among the oceanic

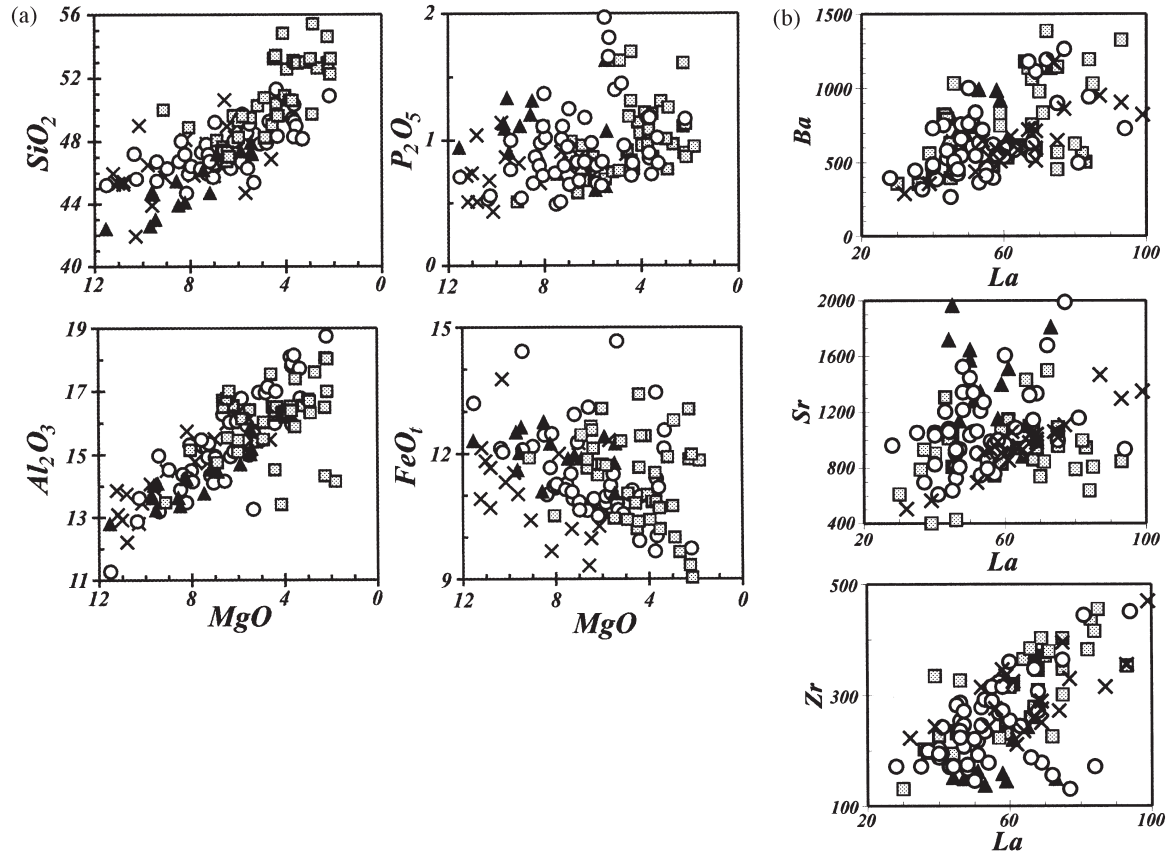

Fig. 4. Major element variations vs MgO (wt %; a) and trace variations vs La (ppm; b), of Western Highlands (Mts Bambouto and Oku) basanite suites (▲), alkali basalt suites (○) and transitional basalt suites (grey squares), as well as of Ngaoundere Plateau basaltic rocks (×).

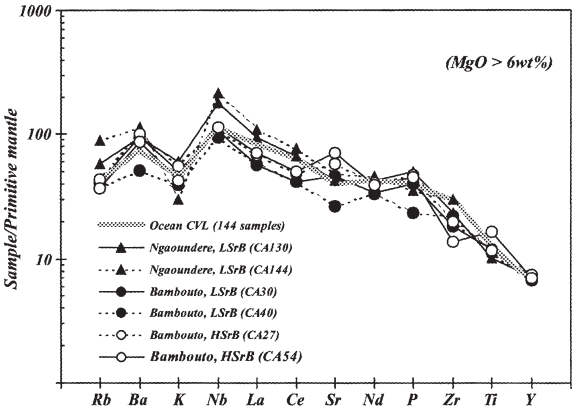

Fig. 5. Primitive mantle normalized (Wood *et al.*, 1979) incompatible element concentrations of representative primitive (MgO > 6 wt %) Western Highlands low-Sr basalts (LSrB) and high-Sr basalts (HSrB), and Ngaoundere basaltic rocks. Mean composition of CVL oceanic basalts (MgO > 4 wt %; Fitton & Dunlop, 1985) is shown for comparison.

CVL basalts, which, instead, are compositionally close to the LSrB of the CVL continental rocks (Fig. 5).

All the analysed samples have steep chondrite-normalized REE patterns [$(La/Yb)_{cn}$ = 7–30; Fig. 7; Table 2], suggesting that they may have been generated by low melting degrees of a garnet peridotite mantle source. Consistently, the highest LREE/HREE (heavy REE) ratios are generally shown by BSN samples. BSN and AKB samples for the Ngaoundere Plateau have $(La/Yb)_{cn}$ slightly higher (23–28 and 13–30, respectively) than the corresponding rocks from the Western Highlands (15–18 and 12–16, respectively). In general, there is a tendency for the REE concentrations to increase with differentiation, whereas LREE/HREE ratios remain virtually constant. An exception is represented by the evolved Bangangte mugearites (Bambouto area, e.g. CA74; Fig. 7c), which have distinct REE patterns with low $(La/Yb)_{cn}$ (6·82).

Sr and Nd isotopic data

In general, the investigated basalts yielded initial $^{87}Sr/^{86}Sr$ (0·70288–0·70382) and initial $^{143}Nd/^{144}Nd$ (0·51292–0·51284, ε_{Nd} +3·7 to +5·6; Fig. 8a, Table 2) that reflect

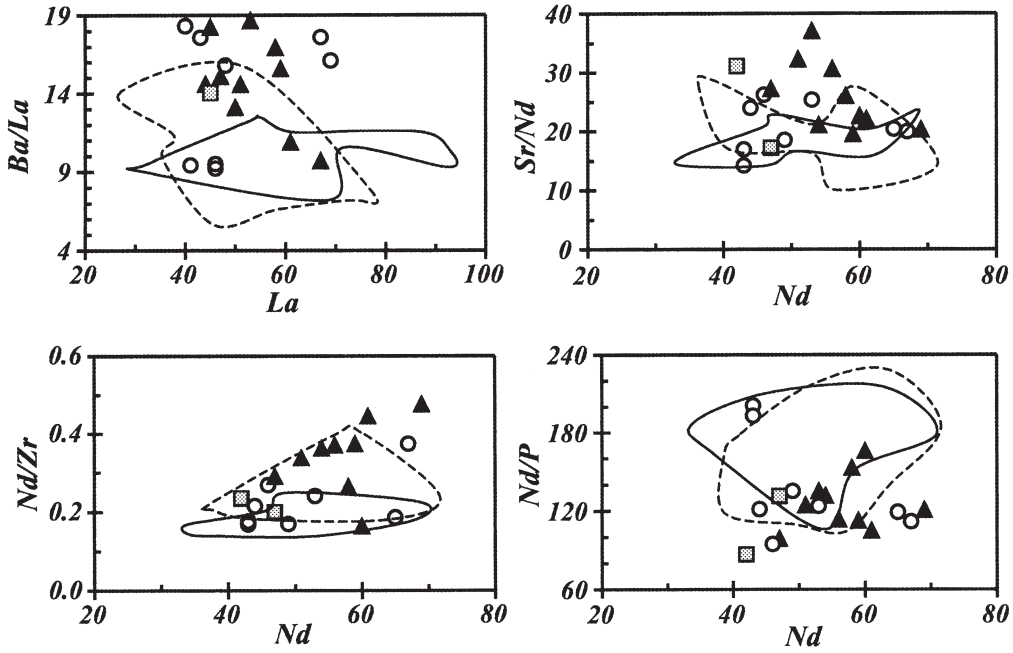

Fig. 6. Variations of incompatible trace element concentrations vs ratios for Mt Bambouto primitive basaltic rocks (MgO > 6 wt %). Dashed and continuous contour fields refer to Mt Oku and Ngaoundere basaltic rocks, respectively.

time-integrated depleted source mantle compositions, and are similar to those of other CVL continental and oceanic basalts (Fitton & Dunlop, 1985; Halliday *et al.*, 1988, 1990). Only a few of the most evolved rocks, i.e. mugearites from Mt Bambouto (CA13, CA73 and CA74), yielded relatively high initial $^{87}Sr/^{86}Sr$ (0·70504–0·70775) and low initial $^{143}Nd/^{144}Nd$ (0·512614–0·512498, ε_{Nd} −0·4 and −2·6; Fig. 8a). Finally, we note that initial $^{87}Sr/^{86}Sr$ compositions of Mt Bambouto samples are slightly variable, with basanites having higher Sr isotopic composition (0·70350–0·70364) than alkali basalts (0·70311–0·70342). In general, initial $^{87}Sr/^{86}Sr$ values of HSr basalts are higher than those of LSr basalts (Fig. 8b), whereas Nd isotopic compositions are indistinguishable.

PETROGENESIS

Fractional crystallization

The petrography, mineral chemistry, and major and trace element variations suggest that differentiation of the basanite (BSN), alkali basalt (AKB) and transitional basalt (TRB) suites is compatible with fractional crystallization at low pressure. The BSN suite is dominated by olivine, clinopyroxene and subordinate magnetite removal; the AKB suite by clinopyroxene, olivine and subordinate magnetite fractionation, and plagioclase during the late stages of evolution; whereas the TRB suite probably differentiated through olivine, clinopyroxene, plagioclase, and moderate magnetite fractionation.

The fractional crystallization model was further tested by using the MELTS code of Ghiorso & Sack (1995). MELTS allows the modelling of liquid lines of descent of silicate magmas as a function of P, T, fO_2 and H_2O, and provides the compositions of both the derivative magmas and liquidus minerals. As an example, the modelled dry and hydrous (H_2O = 1·0 wt %) differentiation trends for Mt Bambouto AKB are shown in Fig. 9. In general, for all suites the best match between modelled and observed differentiation trends and mineralogical compositions was obtained for P_t = 2–4 kbar, H_2O = 0·5–1·5 wt % and fO_2 = QFM (TRB and AKB) and QFM + 1 log unit (BSN). These fO_2 values are consistent with the analysed Fe–Ti oxide compositions (Table 3d) and with literature data for alkali basalts (e.g. Dixon *et al.*, 1997). The crystallization temperatures of coexisting olivine–clinopyroxene phenocrysts calculated for a total pressure <4 kbar using MELTS modelling are virtually the same as those obtained (Table 3b) following Loucks (1996), except for few alkali basalts (Fig. 10).

The MELTS-modelled fractional crystallization process (Fig. 10) from the least evolved basanites to phonotephritic compositions (P = 2–4 kbar, fO_2 = QFM + 1 log unit, H_2O = 1 wt %) requires ~50 wt % fractionation of an assemblage comprising olivine (27 wt %), clinopyroxene (64 wt %), magnetite (7 wt %) and apatite (2 wt %). The transition (2 kbar, QFM, H_2O = 1·0 wt %)

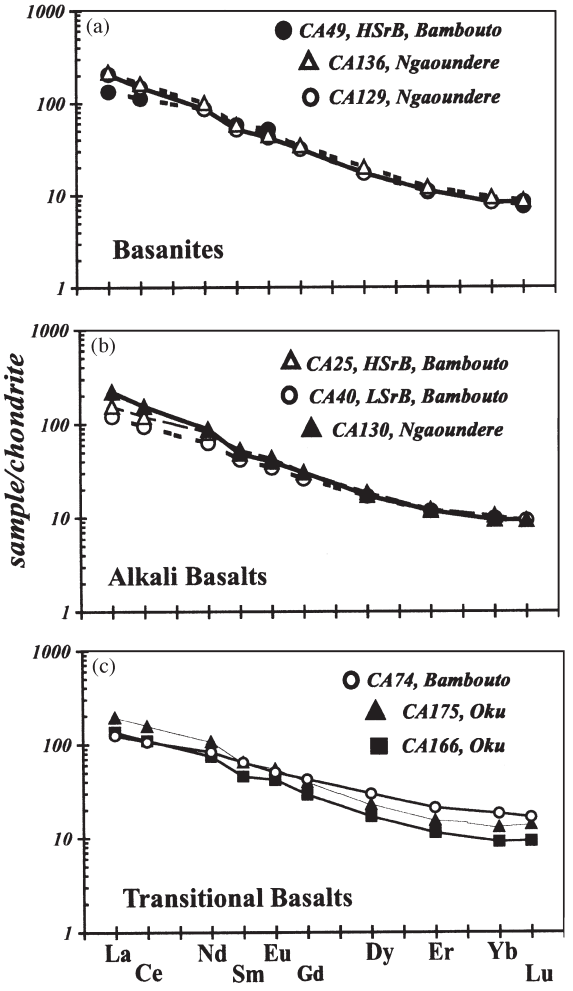

Fig. 7. Chondrite-normalized (Boynton, 1984) REE concentrations of representative basanites (a), alkali basalts (b) and transitional basaltic (TRB; c) rocks from Mt Bambouto, Ngaoundere and Mt Oku (Jakiri lava sequence).

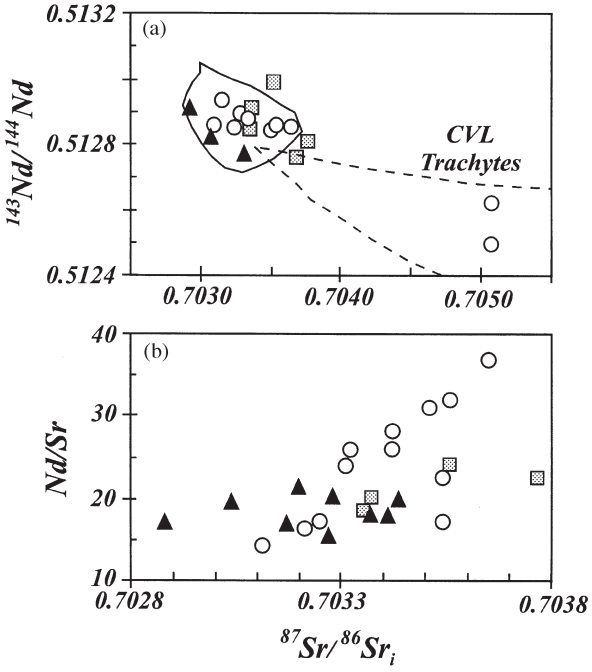

Fig. 8. Initial $^{87}Sr/^{86}Sr$ vs initial $^{143}Nd/^{144}Nd$ (a), and vs Nd/Sr of Mt Bambouto (○), Mt Oku (grey squares) and Ngaoundere (▲) basaltic rocks (b). In (a) isotopic compositions of continental and oceanic CVL basalts (continuous contour field; Halliday *et al.*, 1988, 1990; Lee *et al.*, 1994*a*; Ballentine *et al.*, 1997) and of continental CVL silicic rocks (dashed contour field; Marzoli *et al.*, 1999) are shown for comparison.

from primitive alkali basalts to mugearites may result from ~40 wt % fractionation involving clinopyroxene (57 wt %), olivine (19 wt %), plagioclase (12 wt %), and magnetite (12 wt %). The Hy-normative mugearites may derive from transitional basalts at 2 kbar, fO_2 = QFM and H_2O = 0·5 wt %, through about 60 wt % fractionation involving olivine (16 wt %), clinopyroxene (27 wt %), plagioclase (36 wt %), magnetite (12 wt %) and apatite (1 wt %). Notably, early plagioclase fractionation is exclusive to the transitional basalt suites. These results are consistent with major element mass balance calculations (Stormer & Nicholls, 1978), and with trace element Rayleigh fractionation modelling.

Although it is possible to model the mineralogy and liquid lines of descent of the rocks from the BSN, AKB and TRB suites, the compositional variations within each suite require different parental magmas. For example, the calculated differentiation sequence of a typical LSr alkali basalt (e.g. CA40; Ne = 6, MgO = 8 wt %) shows that the differences between HSr- and LSr-type basalts cannot be explained through fractional crystallization, even assuming different P and fO_2 conditions and H_2O contents (Fig. 9). Similarly, the compositional differences between the rocks of Mt Bambouto and Ngaoundere Plateau demand different parental magmas.

Crustal contamination

Crustal contamination may be important in alkali basalt petrogenesis (e.g. Wilson *et al.*, 1995), despite the high ascent velocity of the parental magmas. The broad similarity between CVL oceanic and continental basalts (Fitton & Dunlop, 1985) and their unradiogenic Sr and radiogenic Nd isotopic compositions (Halliday *et al.*, 1988) suggest that crustal contamination was probably negligible.

However, a few evolved basaltic rocks, i.e. quartz-normative Bangangte mugearites (e.g. CA74, 42 Ma) and one Hy mugearite (CA13), from the Bambouto area, have isotopic compositions that fall far from the CVL

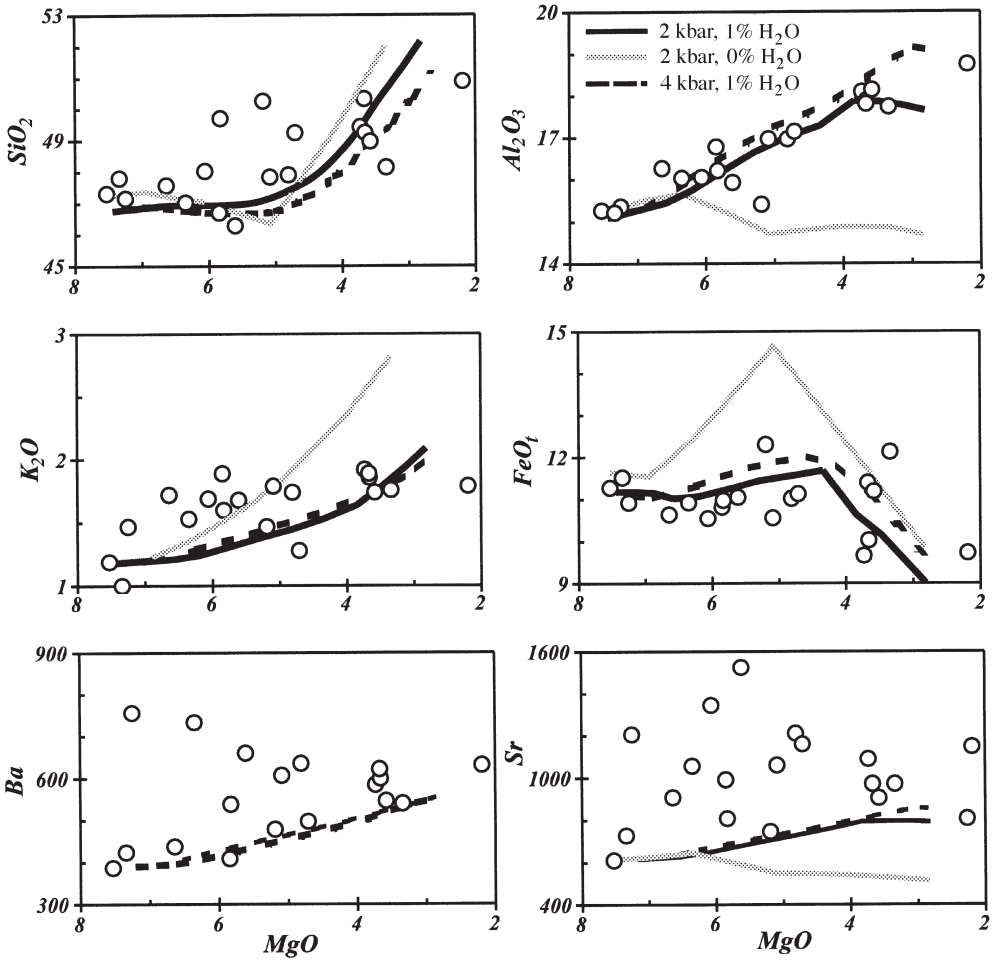

Fig. 9. Calculated fractional crystallization trends for major (wt %; MELTS modelling; Ghiorso & Sack, 1995) and trace elements (ppm; Rayleigh fractionation equation) compared with compositions of AKB samples from Mt Bambouto (○). Starting magma composition is the aphyric alkali basalt CA40 (Table 2). H_2O contents refer to the starting magma composition. fO_2 corresponds to the QFM buffer. For trace elements, fractionating minerals and fraction of residual liquid are calculated by MELTS (see Fig. 10), and partition coefficients are from LeMarchand *et al.* (1987).

basaltic field (Fig. 8a), i.e. they have high initial $^{87}Sr/^{86}Sr$ (0·70500–0·70775) and low initial $^{143}Nd/^{144}Nd$ (0·51257–0·512499). These isotopic compositions, coupled with relatively high SiO_2 (53–55 wt %) and relatively low Nb (39–89 ppm) may be indicative of contamination with silicic crustal material, possibly the Pan-African granites of the basement. These granitoids are characterized by high SiO_2 (64–77 wt %), low Nb (~30 ppm), high $^{87}Sr/^{86}Sr$ (0·71043–0·72099) and low $^{143}Nd/^{144}Nd$ (0·51215–0·51165; Halliday *et al.*, 1988; Marzoli *et al.*, 1999; A. Marzoli, unpublished data, 1999). The relatively low LREE/HREE ratio of the mugearite CA74 [$(La/Yb)_{CN}$ = 6·82], compared with the high ratios of associated basalts [$(La/Yb)_{CN}$ = 12–30; Fig. 7], is compatible with the assimilation of basement Pan-African granites that have $(La/Yb)_{CN}$ = 4–7 (Toteau, 1990). An assimilation–fractional crystallization process (AFC; DePaolo, 1981) can explain the high Sr and low Nd isotopic values of the Bangangte mugearites, starting from the transitional basalt CA4, and assuming granite CA18 (Marzoli *et al.*, 1999) as contaminant, with an *r* value (i.e. rate of assimilated mass/rate of fractionated mass) of 0·3.

In contrast, AFC modelling was not successful in explaining differences between HSrB and LSrB compositions. Common crustal materials are not suitable to change the concentrations of Ba, Sr and P significantly, without substantially affecting major and other trace elements. In summary, crustal contamination is not appreciable in most of the investigated basaltic rocks of the CVL continental sector.

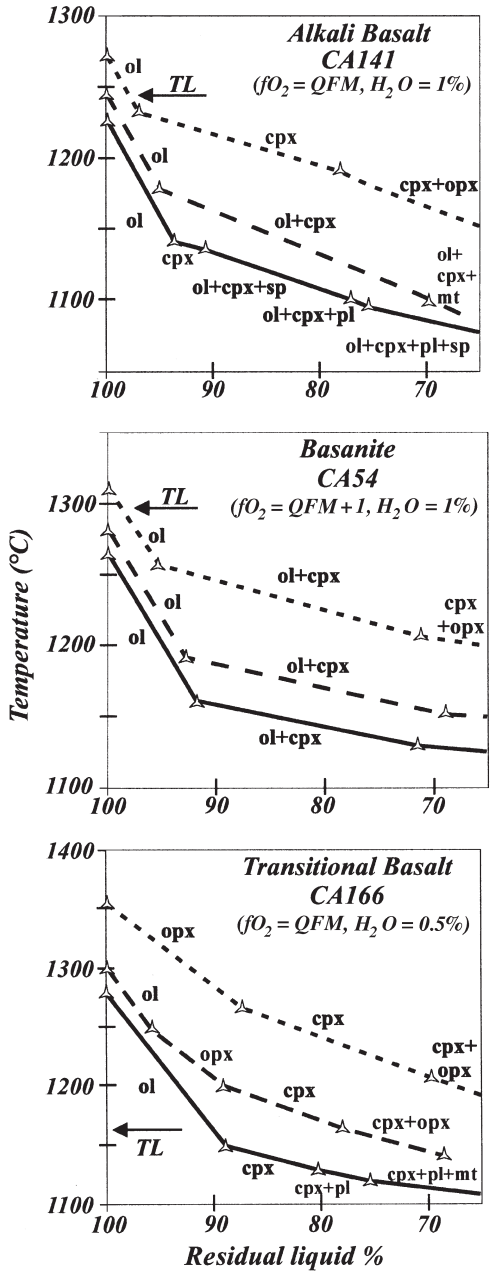

Fig. 10. Liquidus temperatures (°C) and fractionating mineral assemblages calculated by MELTS as a function of residual liquid mass for primitive, slightly porphyritic, alkali basalt (CA141), basanite (CA54) and transitional basalt (CA166; Table 2). Liquidus curves are calculated for 2 kbar (continuous line), 4 kbar (dashed lines) and 8 kbar (dotted lines). ol, olivine; cpx, clinopyroxene; mt, magnetite; pl, plagioclase; opx, orthopyroxene; sp, spinel; TL, calculated clinopyroxene–olivine pair crystallization temperature (Loucks, 1996; see Table 3b).

Lithospheric and asthenospheric mantle sources

About 10% of the analysed CVL basaltic rocks have compositions that approach those of primary melts (*mg*-number values 0·60–0·68; Ni 86–321 ppm; Cr 200–493 ppm; see Table 2). In general, primitive (MgO > 7 wt %) basanites and alkali basalts of Ngaoundere are depleted in FeO_t and slightly enriched in SiO_2 (Fig. 4a), and have generally higher LREE/HREE ratios than the Western Highlands volcanics with similar MgO (Fig. 7). These differences cannot be due only to fractional crystallization of olivine and clinopyroxene (see Figs 9 and 10). High-pressure experiments on dry lherzolites (e.g. Adam, 1990; Hirose & Kushiro, 1993; Green & Falloon, 1998) suggest that the SiO_2 concentration of mantle partial melts are pressure and temperature (i.e. melting degree) dependent, whereas FeO_t concentrations are mainly pressure dependent (i.e. increasing with pressure). Therefore, we suggest that Ngaoundere basanites and alkali basalts may have been generated at lower pressure than Bambouto ones. This is consistent with geophysical evidence that the lithosphere is thinned beneath the Ngaoundere Plateau (Plomerova *et al.*, 1993; Poudjom Djomani *et al.*, 1995, 1997). Mt Bambouto basanites are relatively depleted in SiO_2 and have high LREE/HREE, compared with Mt Bambouto alkali basalts, whereas FeO_t concentrations are similar (Figs 4a and 7; Table 2). We interpret these compositional differences between basanites and alkali basalts to reflect essentially increasing melting degrees.

Incompatible trace element ratios in the least evolved basaltic samples were considered, to provide further constraints on their mantle source(s). REE modelling shows that the least evolved CVL volcanics (basanites, alkali basalts and transitional basalts) fall between the equilibrium batch melting curve for a depleted garnet lherzolite and that for an amphibole–garnet lherzolite with primitive mantle concentrations (Fig. 11a).

CVL basalts of the oceanic sector (Fitton & Dunlop, 1985), of the Ngaoundere Plateau, and LSrB from Mts Oku and Bambouto have similar incompatible element patterns, suggesting that they were generated in the asthenospheric mantle. Their Rb to Y concentrations are similar to those derived by 0·5–1% melting of a depleted garnet lherzolite (McKenzie & O'Nions, 1991; Fig. 11b).

The incompatible element patterns of the basaltic volcanics of HSr type, instead, are exclusive to the continental sector, and approach those of modelled low-degree (1%) melts of an amphibole-bearing garnet lherzolite (Fig. 11c). Compared with the depleted mantle source of the LSrB, the mantle source of HSrB must have been rich in Sr (~40 ppm) and Ba (~14 ppm), and slightly depleted in Zr (~3·0 ppm), and trace amounts of apatite (<1 wt %) in the mantle source of HSrB could account for their high P_2O_5 concentrations (not shown in Fig. 11). The Sr–Nd isotopic compositions of HSr and LSr rocks suggest that the HSr mantle component was slightly enriched

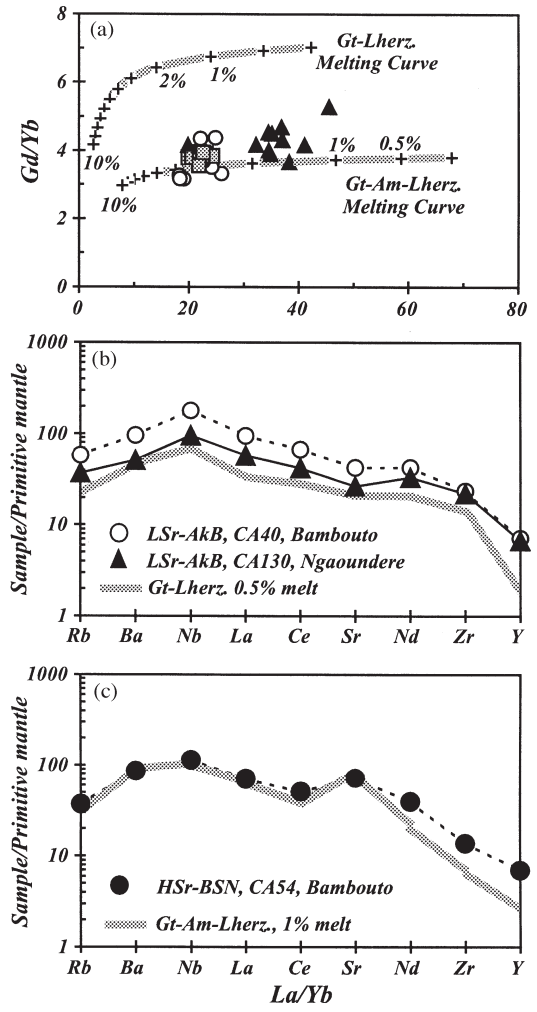

Fig. 11. (a) La/Yb vs Gd/Yb variations as a function of degree of equilibrium melting (0·2, 0·5, 1, 2, 3%, etc.) of garnet lherzolites and garnet–amphibole lherzolites. Symbols for CVL basaltic rocks (MgO > 7 wt %): grey squares, Mt Oku; ○, Mt Bambouto; ▲, Ngaoundere. Incompatible element depleted garnet lherzolite and primitive garnet–amphibole lherzolite compositions are from McKenzie & O'Nions (1991) and Ionov *et al.* (1996), respectively. Partition coefficients for olivine, pyroxenes and garnet are from McKenzie & O'Nions (1991), and those for amphibole are from Adam *et al.* (1993) and Adam & Green (1994). Modal and melting proportions for garnet lherzolite are from McKenzie & O'Nions (1991). For garnet–amphibole lherzolite, modal proportions and melting coefficients are respectively: olivine 0·55 and 0·05; orthopyroxene 0·19 and 0·11; clinopyroxene 0·07 and 0·25; garnet 0·08 and 0·20; amphibole 0·11 and 0·40. (b, c) Primitive mantle normalized (Wood *et al.*, 1979) incompatible element concentrations of primary melts calculated for 0·5% and 1% equilibrium melting compositions, starting from a garnet lherzolite (Gt-Lherz.) and a garnet–amphibole lherzolite (Gt–Am-Lherz.), compared with compositions of representative primitive (MgO > 7 wt %) low-Sr alkali basalts (LSr-AkB; Western Highlands and Ngaoundere), and high-Sr basanites (HSr-BSN; Western Highlands), respectively.

in $^{87}Sr/^{86}Sr$, but similar in $^{143}Nd/^{144}Nd$ isotopic composition to the LSr component (Fig. 8).

It should be noted that amphibole-bearing peridotite xenoliths were found in Western Highlands (A. Marzoli, unpublished data, 1999) and in Ngaoundere Plateau volcanics (Lee *et al.*, 1996). The amphiboles in these mantle xenoliths are characterized by positive Ba and Sr anomalies, and by relatively enriched LREE concentrations (Lee *et al.*, 1996). Considering the low P–T stability of amphibole (<30 kbar and <1050°C; see Mengel & Green, 1989; Foley, 1991) and of apatite (Watson, 1980; Baker & Willey, 1992), and considering the ~100 km lithospheric thickness (e.g. Plomerova *et al.*, 1993), the amphibole-related chemical signature of the continental CVL magmas suggests a lithospheric mantle source component in the petrogenesis of these HSr basalts. As Western Highlands basalts represent a continuous spectrum from HSr to LSr compositions, we suggest that they may result from mixing of variable amounts of asthenospheric melts derived from an incompatible element depleted anhydrous lherzolite (i.e. LSr component) and of 'small-volume' melts from amphibole-bearing lithospheric mantle peridotite (i.e. HSr component).

Mantle enrichment

Incompatible element modelling suggests that the amphibole- and apatite-bearing mantle source of HSrB was enriched in Sr and Ba, and depleted in Zr. Typically, mantle lherzolites affected by carbonate (CO_2-rich fluids or carbonatitic magmas) metasomatism may contain amphibole and sometimes apatite, and are characterized by amphibole (and clinopyroxene) enriched in Sr and Ba, and depleted in Zr (e.g. Ionov *et al.*, 1996). It is possible that carbonate metasomatism may have affected the lithospheric mantle source of Mt Bambouto HSrB (and of Mt Etinde nephelinites; Nkoumbo *et al.*, 1995), allowing for Ba, Sr and P enrichments and Zr depletion. As (carbonate) metasomatism produces generally enriched LREE/HREE ratios (e.g. Ionov *et al.*, 1996), a relatively recent enrichment process would be consistent with the $^{143}Nd/^{144}Nd$ isotopic data, which show no variation between HSrB and LSrB and require a time-integrated LREE-depleted source.

Although the age, origin and nature of the metasomatic event that possibly affected the mantle source of the continental HSrB remains poorly constrained, a Mesozoic enrichment may be hypothesized according to studies on CVL mantle xenoliths and on basalts from the continent–ocean boundary region (Halliday *et al.*, 1990; Lee *et al.*, 1994*a*, 1996). The CVL mantle xenoliths show evidence of Mesozoic incompatible element enrichments (Lee *et al.*, 1996), which may be related to the activity of the St Helena hotspot. During the Early Cretaceous, the St Helena hotspot was located underneath the Benue Trough, where it generated alkali basaltic magmatism

~200 km to the north of the Western Cameroon Highlands (Coulon *et al.*, 1996). Subsequently, the hotspot migrated towards the region at present located underneath southern Cameroon and Nigeria (O'Connor & Le Roex, 1992), where the anomalously high Pb isotopic compositions of the CVL basalts at the continent–ocean boundary, including the HSr Mt Etinde nephelinites (Halliday *et al.*, 1990; Lee *et al.*, 1994*a*), provide further record of a Mesozoic enrichment event. It may be suggested that magmas or fluids associated with the St Helena mantle plume and the Early Cretaceous alkaline magmatism in the Benue Trough enriched the continental mantle lithosphere, which became later the source of the HSr basalts at the continental–ocean boundary (Mt Etinde) and in the Western Highlands. This scenario is consistent with the absence of HSr basalts on the Ngaoundere Plateau, which was too far from the location of the hotspot, and in the CVL oceanic sector, as no oceanic crust was formed before the Late Cretaceous in the Equatorial Atlantic.

In summary, low degrees of partial melting of a dry, depleted, lherzolite asthenospheric mantle source can account for the common signature of the oceanic and continental CVL basalts, whereas the anomalous chemical characteristics of HSrB, exclusive to CVL continental basalts, suggest the involvement of a metasomatically enriched, amphibole- (and apatite-)bearing lherzolite from the continental lithosphere.

SW MIGRATION OF THE VOLCANISM AND PLATE MOTION

The $^{40}Ar/^{39}Ar$ ages of the silicic volcanism of the Western Highlands (Marzoli *et al.*, 1999) and the age of the peak basaltic activity at Mt Oku (Ndu, 31–23 Ma, to Bamenda, 25–15 Ma; Njilah, 1991) and Mt Bambouto (21–14 Ma) are consistent with a general SW younging of the volcanism in the Western Highlands. Previous K/Ar data (Gouhier *et al.*, 1974; Fitton & Dunlop, 1985) suggested that this younging trend extends to all the NE–SW aligned continental Cameroon volcanoes, from the Oligocene Mandara volcanic mountains (northern Cameroon) to the mainly Pliocene–Quaternary volcanism of Mts Manengouba, Cameroon and Etinde, and of Bioko island (southwest Cameroon; Fig. 1). K/Ar ages of intrusive rocks of northern Cameroon (e.g. Golda Zuelva and Mboutou, 66–55 Ma; Jacquemin *et al.*, 1982) are broadly consistent with the above NE–SW trend.

Notably, the African plate moved from SW to NE with a velocity of ~1·5–2 cm/y in Oligocene–Pliocene times (Pollitz, 1991; Silver *et al.*, 1998; Ubangoh *et al.*, 1998). It is therefore suggested that the peak magmatic activity in the continental sector of the CVL migrated to the SW, as a response to the NE movement of the African plate above a deep-seated thermal anomaly. This is consistent with the general tendency of the Western Highlands volcanism to become more alkaline with time. Also, the transition in the Western Highlands from early LSrB, generated by melting of a depleted asthenospheric mantle, to late HSrB, generated by melting low-temperature components (e.g. amphibole) of the enriched lithospheric mantle, indicates a progressive decline of the melting degree.

In contrast, several lines of evidence suggest that the whole CVL cannot be considered the expression of a simple hotspot system, as, for example, the Hawaiian islands: (1) the SW-younging volcanism in the continental sector parallels that of the onset of basaltic volcanism in the CVL oceanic sector, i.e. from Principe (31 Ma) to Pagalu (5 Ma) islands (Lee *et al.*, 1994*a*), requiring an independent mantle thermal anomaly. (2) Eocene to Oligocene intrusive complexes in southwestern Cameroon (Cantagrel *et al.*, 1978) and the Miocene to Quaternary volcanism of the Ngaoundere plateau in northeastern Cameroon do not conform to the general NE–SW younging trend. (3) Magmatism persisted on single continental volcanoes (e.g. Mts Oku and Bambouto) and volcanic islands (Principe; Lee *et al.*, 1994a) for as much as 30 My, requiring a long persistence of the mantle thermal anomaly and a strong tectonic control on the location of the volcanism.

However, the data presented in this study for the continental CVL, and those of Lee *et al.* (1994*a*) for the oceanic CVL, support the idea of a Oligocene to Quaternary NE–SW extending mantle hotline (Meyers *et al.*, 1998), within which distinct thermal anomalies were responsible for the CVL oceanic and continental magmatism during the NE movement of the African plate.

ACKNOWLEDGEMENTS

We are grateful to A. Cundari and E. M. Iarap for helpful discussions of an earlier version of the manuscript. Critical reviews by J. G. Fitton, A. N. Halliday, M. Wilson and an anonymous reviewer substantially improved the manuscript and are gratefully acknowledged. We thank L. Furlan and R. Zettin (Trieste), A. Giaretta and R. Carampin (Padua), and T. Becker (Berkeley) for their technical and analytical collaboration. Financial support from Italian (CNR and MURST) and Brazilian agencies (PADCT/FINEP) is gratefully acknowledged. Geochronology studies at Berkeley Geochronology Center were supported by the Ann and Gordon Getty Foundation.

REFERENCES

Adam, J. (1990). The geochemistry and experimental petrology of sodic alkaline basalts from Oatlands, Tasmania. *Journal of Petrology* **31**, 1201–1223.

Adam, J. & Green, T. H. (1994). The effects of pressure and temperature on the partitioning of Ti, Sr and REE between amphibole, clinopyroxene and basanitic melts. *Chemical Geology* **117**, 219–234.

Adam, J., Green, T. H. & Sie, S. H. (1993). Proton microprobe determined partitioning of Rb, Sr, Ba, Y, Zr, Nb, and Ta between experimentally produced amphiboles and silicate melts. *Chemical Geology* **109**, 29–49.

Baker, D. K. & Willey, P. J. (1992). High pressure apatite solubility in carbonate-rich liquids: implications for mantle metasomatism. *Geochimica et Cosmochimica Acta* **56**, 3409–3422.

Ballentine, C. J., Lee, D. C. & Halliday, A. N. (1997). Hafnium isotopic studies of the Cameroon line and new HIMU paradoxes. *Chemical Geology* **139**, 111–124.

Boynton, W. V. (1984). Cosmochemistry of rare earth elements: meteorite studies. In: Henderson, P. (ed.) *Rare Earth Element Geochemistry*. Amsterdam: Elsevier, pp. 63–114.

Browne, S. & Fairhead, J. D., 1983. Gravity study of the central African rift system: a model of continental disruption. 1. The Ngaoundere and Abu Gabra rifts. *Tectonophysics* **132**, 103–115.

Cantagrel, J. M., Jamond, C. & Lassere, M. (1978). Le magmatism alcalin de la ligne du Cameroun au Tertiaire inférieur: données géochronologiques K/Ar. *Comptes Rendus Sommaire de la Société Géologique de France* **6**, 300–303.

Chazot, G., Menzies, M. A. & Harte, B. (1996). Determination of partition coefficients between apatite, clinopyroxene, amphibole, and melt in natural spinel lherzolites from Yemen: implications for wet melting of the lithospheric mantle. *Geochimica et Cosmochimica Acta* **60**, 423–437.

Class, C. & Goldstein, S. L. (1997). Plume–lithosphere interactions in the ocean basins: constraints from the source mineralogy. *Earth and Planetary Science Letters* **150**, 245–260.

Comin-Chiaramonti, P., Cundari, A., Piccirillo, E. M., Gomes, C. B., Castorina, F., Censi, P., De Min, A., Marzoli, A., Speziale, S. & Velázquez, V. F. (1997). Potassic and sodic igneous rocks from eastern Paraguay: their origin from a lithospheric mantle and genetic relationships with the associated Paranà flood tholeiites. *Journal of Petrology* **38**, 495–528.

Coulon, C., Vidal, P., Dupuy, C., Baudin, P., Popoff, M., Maluski, H. & Hermitte, D. (1996). The Mesozoic to Early Cenozoic magmatism of the Benue Trough (Nigeria); geochemical evidence for the involvement of the St Helena plume. *Journal of Petrology* **37**, 1341–1358.

DePaolo, D. J. (1981). Trace element and isotopic effects of combined wallrock assimilation and fractional crystallization. *Earth and Planetary Science Letters* **53**, 189–202.

Déruelle, B., Moreau, C., Nkoumbou, C., Kambou, R., Lissom, J., Njofang, E. & Nono, A. (1991). The Cameroon Line: a review. In: Kampunzu, A. B. & Lubala, R. T. (eds) *Magmatism in Extensional Tectonic Structural Settings*. Berlin: Springer, pp. 274–327.

Dixon, J. E., Clague, D. A., Wallace, P. & Poreda, R. (1997). Volatiles in alkalic basalts from the North Arch volcanic field, Hawaii: extensive degassing of deep submarine-erupted alkalic series lavas. *Journal of Petrology* **38**, 911–939.

Fairhead, J. D. & Binks, R. M. (1991). Differential opening of the Central and South Atlantic and the opening of the West African Rift system. *Tectonophysics* **187**, 191–203.

Fairhead, J. D. & Okereke, C. S. (1987). A regional study of the West African Rift system in Nigeria and Cameroon and its tectonic interpretation. *Tectonophysics* **143**, 141–159.

Fitton, J. G. (1987). The Cameroon Line, West Africa: a comparison between oceanic and continental alkaline volcanism. In: Fitton, J. G. & Upton, B. G. J. (eds) *Alkaline Igneous Rocks. Geological Society, London, Special Publication* **30**, 273–291.

Fitton, J. G. & Dunlop, H. M. (1985). The Cameroon Line, West Africa, and its bearing on the origin of oceanic and continental alkalic basalt. *Earth and Planetary Science Letters* **72**, 23–38.

Foley, S. (1991). High-pressure stability of the fluor- and hydroxyl-endmembers of pargasite and K-richterite. *Contributions to Mineralogy and Petrology* **55**, 2689–2694.

Francis, D. & Ludden, J. (1995). The signature of amphibole in mafic alkaline lavas, a study in the northern Canadian Cordillera. *Journal of Petrology* **36**, 1171–1191.

Ghiorso, M. S. & Sack, R. O. (1995). Chemical mass transfer in magmatic processes IV. A revised and internally consistent thermodynamic model for the interpolation and extrapolation of liquid–solid equilibria in magmatic systems at elevated temperatures and pressures. *Contributions to Mineralogy and Petrology* **119**, 197–212.

Gouhier, J., Nougier, J. & Nougier, D. (1974). Contribution à l'étude volcanologique du Cameroun ('Ligne du Cameroun'–Adamaoua). *Annales de la Faculté des Sciences, Université de Yaoundé, Cameroun* **17**, 69–78.

Govindaraju, K. & Mevelle, G. (1987). Fully automated dissolution and separation methods for inductively coupled plasma atomic emission spectrometry rock analysis. Application to the determination of rare earth elements. *Journal of Analytical Atomic Spectrometry* **2**, 615–621.

Green, D. H. & Falloon, T. J. (1998). Pyrolite: a Ringwood concept and its current expression. In: Jackson, I. (ed.) *The Earth's Mantle*. Cambridge: Cambridge University Press, pp. 311–378.

Halliday, A. N., Dickin, A. P., Fallick, A. E. & Fitton, J. G. (1988). Mantle dynamics: a Nd, Sr, Pb and O isotopic study of the Cameroon line volcanic chain. *Journal of Petrology* **29**, 181–211.

Halliday, A. N., Davidson, J. P., Holden, P., DeWolf, C. P., Lee, D. C. & Fitton, J. G. (1990). Trace element fractionation in plumes and the origin of HIMU mantle beneath the Cameroon Line. *Nature* **347**, 523–528.

Hirose, K. & Kushiro, I. (1993). Partial melting of dry peridotites at high pressures: determination of compositions of melts segregated from peridotite using aggregates of diamond. *Earth and Planetary Science Letters* **114**, 477–489.

Hofmann, A. W. (1988). Chemical differentiation of the Earth: the relationship between mantle, continental crust, and oceanic crust. *Earth and Planetary Science Letters* **90**, 297–314.

Ionov, D. A., O'Reilly, S. Y., Genshaft, Y. S. & Kopylova, M. G. (1996). Carbonate-bearing mantle peridotite xenoliths from Spitsbergen: phase relationships, mineral compositions and trace-element residence. *Contributions to Mineralogy and Petrology* **125**, 375–392.

Jacquemin, H., Sheppard, S. M. F. & Vidal, P. (1982). Isotope geochemistry (O, Sr, Pb) of the Golda Zuelva and Mboutou anorogenic complexes, North Cameroon: mantle origin with evidence for crustal contamination. *Earth and Planetary Science Letters* **61**, 97–111.

Lassere, M. (1978). Mise au point sur les granitoïds dits 'ultimes' du Cameroun. Gisements, pétrographie et géochronologie. *Bulletin du Bureau de Recherches Géologiques et Minières* **2**(4), 143–159.

Le Bas, M. J., Le Maitre, R. W., Streckeisen, A. & Zanettin, B. (1986). Chemical classification of volcanic rocks based on the total alkali–silica diagram. *Journal of Petrology* **27**, 745–750.

Lee, D. C, Halliday, A. N., Fitton, J. G. & Poli, G. (1994*a*). Isotopic variations with distance and time in the volcanic islands of the Cameroon line: evidence for a mantle plume origin. *Earth and Planetary Science Letters* **123**, 119–138.

Lee, D. C., Halliday, A. N., Hall, C. M. & Fitton, J. G. (1994*b*). Similarities and differences between continental and oceanic basalts in the Cameroon Line. *Eighth International Conference on Geochronology, Cosmochronology and Isotope Geology, Berkeley*. Denver, CO: US Geological Survey Circular 1107, p. 188.

Lee, D. C., Halliday, A. N., Davies, G. R., Essene, E. J., Fitton, J. G. & Temdjim, R. (1996). Melt enrichment of shallow depleted mantle: a detailed petrological, trace element and isotopic study of mantle-derived xenoliths and megacrysts from the Cameroon Line. *Journal of Petrology* **38**, 415–441.

LeMarchand, F., Villemant, B. & Calas, G. (1987). Trace element distribution coefficients in alkaline series. *Geochimica et Cosmochimica Acta* **51**, 1071–1081.

Loucks, R. R. (1996). A precise olivine–augite Mg–Fe-exchange geothermometer. *Contributions to Mineralogy and Petrology* **125**, 140–150.

Maluski, H., Coulon, C., Popoff, M. & Baudin, P. (1995). $^{40}Ar/^{39}Ar$ chronology, petrology and geodynamic setting of Mesozoic to Early Cenozoic magmatism from the Benue Trough, Nigeria. *Journal of the Geological Society, London* **152**, 311–326.

Marzoli, A., Renne, P. R., Piccirillo, E. M., Castorina, F., Bellieni, G., Melfi, A. J., Nyobe, J. B. & N'ni, J. (1999). Silicic magmas from the continental Cameroon volcanic line (Oku, Bambouto and Ngaoundere): $^{40}Ar/^{39}Ar$ dates, petrology, Sr–Nd–O isotopes and their petrogenetic significance. *Contributions to Mineralogy and Petrology* **135**, 133–150.

Mathez, E. A. (1973). Refinement of the Kudo–Weil plagioclase thermometer and its application to basaltic rocks. *Contributions to Mineralogy and Petrology* **41**, 61–72.

McKenzie, D. & O'Nions, R. K. (1991). Partial melt distribution from inversion of rare earth element concentrations. *Journal of Petrology* **32**, 1021–1091.

McKenzie, D. & O'Nions, R. K. (1995). The source regions of ocean island basalts. *Journal of Petrology* **36**, 133–160.

Mengel, K. & Green, D. H. (1989). Stability of amphibole and phlogopite in metasomatized peridotite under water-saturated and water-undersaturated conditions. In: Ross, J. (ed.) *Kimberlites and Related Rocks. Geological Society of Australia, Special Publication* **14**, 571–581.

Menzies, M. A. & Hawkesworth, C. J. (eds) (1987). *Mantle Metasomatism*. London: Academic Press.

Meyers, J. B., Rosendahl, B. R., Harrison, C. G. A. & Ding, Z. D. (1998). Deep imaging seismic and gravity results from the offshore Cameroon Volcanic Line, and speculation of African hotline. *Tectonophysics* **284**, 31–63.

Moreau, C., Regnoult, J. M., Déruelle, B. & Robineau, B. (1987). A new tectonic model for the Cameroon line, Central Africa. *Tectonophysics* **139**, 317–334.

Nimis, P. (1995). A clinopyroxene geobarometer for basaltic systems based on crystal-structure modelling. *Contributions to Mineralogy and Petrology* **121**, 115–125.

Njilah, I. K. (1991). Geochemistry and petrogenesis of Tertiary–Quaternary volcanic rocks from Oku-Ndu area, N.W. Cameroon. Ph.D. Thesis, University of Leeds.

Nkoumbo, C., Déruelle, B. & Velde, D. (1995). Petrology of Mt Etinde nephelinite series. *Journal of Petrology* **6**, 373–395.

Nono, A., Déruelle, B., Demaiffe, D. & Kambouc, R. (1994). Tchabal Nganha volcano in Adamawa (Cameroon): petrology of continental alkaline lava series. *Journal of Volcanology and Geothermal Research* **60**, 147–177.

O'Connor, J. M. & Le Roex, A. P (1992). South Atlantic hot spot–plume system: 1. Distribution of volcanism in time and space. *Earth and Planetary Science Letters* **113**, 343–364.

Ottonello, G., Della Giusta, A., Dal Negro, A. & Beccarin, F. (1992). A structure energy model for C2/c pyroxenes in the system Na–Mg–Ca–Mn–Fe–Al–Cr–Ti–Si–O. In: Saxena, S. K. (ed.) *Advances in Physical Geochemistry, Thermodynamic Data*. Berlin: Springer, pp. 194–238.

Philips (1994). *X40 Software for XRF Analysis. Software Operational Manual*. Eindhoven: Philips, 425 pp.

Plomerova, J., Babuska, V., Dorbath, L. & Lillie, R. (1993). Deep lithospheric structure across the Central African Shear Zone in Cameroon. *Geophysical Journal International* **115**, 381–390.

Pollitz, F. F. (1991). Two stage model of African absolute motion during the last 30 million years. *Tectonophysics* **194**, 91–106.

Poudjom Djomani, Y. H., Nnange, J. M., Diament, M., Ebinger, C. J. & Fairhead, J. D. (1995). Effective elastic thickness and crustal thickness variations in west–central Africa inferred from gravity data. *Journal of Geophysical Research* **100**, 22047–22070.

Poudjom Djomani, Y. H., Diament, M. & Wilson, M. (1997). Lithospheric structure across the Adamawa plateau (Cameroon) from gravity studies. *Tectonophysics* **273**, 317–327.

Renne, P. R. (1995). Excess ^{40}Ar in biotite and hornblende from the Noril'sk 1 intrusion, Siberia: implications for the age of the Siberian Traps. *Earth and Planetary Science Letters* **131**, 165–176.

Renne, P. R., Swisher, C. C., Deino, A. L., Karner, D. B., Owens, T. & DePaolo, D. J. (1998). Intercalibration of standards, absolute ages and uncertainties in $^{40}Ar/^{39}Ar$ dating. *Chemical Geology (Isotope Geoscience Section)* **145**, 117–152.

Roeder, P. L. & Emslie, R. F. (1970). Olivine–liquid equilibrium. *Contributions to Mineralogy and Petrology* **29**, 275–289.

Silver, P. G., Russo, R. M. & Lithgow-Bertelloni, C. (1998). Coupling of South American and African plate motion and plate deformation. *Science* **279**, 60–63.

Smith, A. G. & Livermore, R. A. (1991). Pangaea in Permian to Jurassic time. *Tectonophysics* **187**, 237–243.

Stormer, J. C. & Nicholls, J. (1978). XLFRAC: a program for interactive testing of magmatic differentiation models. *Computers and Geosciences* **4**, 143–159.

Toteau, S. F. (1990). Geochemical characterization of the main petrographical and structural units of northern Cameroon: implications for Pan-African evolution. *Journal of African Earth Sciences* **10**, 615–624.

Toteau, S. F., Van Schmus, W. R., Penaye, J. & Nyobe, J. B. (1994). U–Pb and Sm–Nd evidence for Eburnian and Pan-African high grade metamorphism in cratonic rocks of southern Cameroon. *Precambrian Research* **67**, 321–347.

Ubangoh, R. S., Pacca, I. G. & Nyobe, J. B. (1998). Palaeomagnetism of the continental sector of the Cameroon Volcanic Line, West Africa. *Geophysical Journal International* **135**, 362–374.

Watson, E. B. (1980). Apatite and phosphorus in mantle source regions: an experimental study of apatite/melt equilibria at pressures to 25 kbar. *Earth and Planetary Science Letters* **51**, 322–335.

Wilson, M. & Guiraud, R. (1992). Magmatism in western and central Africa, from Late Jurassic to Recent times. *Tectonophysics* **213**, 203–225.

Wilson, M., Downes, H. & Cebria, J. M. (1995). Contrasting fractionation trends in coexisting continental alkaline magma series; Cantal, Massif Central, France. *Journal of Petrology* **36**, 1729–1753.

Wood, S. D., Joron, J. J., Trueil, M., Norry, M. & Tarney, J. (1979). Elemental and Sr isotope variations in basic lavas from Iceland and surrounding ocean floor. The nature of mantle source heterogeneities. *Contributions to Mineralogy and Petrology* **70**, 319–340.

Wulff-Pedersen, E., Neumann, E. R. & Jensen, B. B. (1996). The upper mantle under La Palma, Canary Islands: formation of Si–K–Na-rich melt and its importance as a metasomatic agent. *Contributions to Mineralogy and Petrology* **125**, 113–139.